

The G-dwarf problem in the Galaxy

R. Caimmi*

November 1, 2018

Abstract

This paper has two parts: one about observational constraints, and the other about chemical evolution models. In the first part, the empirical differential metallicity distribution (EDMD) is deduced from three different samples involving (i) local thick disk stars derived from Gliese and scaled in situ samples within the range, $-1.20 \leq [\text{Fe}/\text{H}] \leq -0.20$ [Wyse, R.F.G., Gilmore, G., 1995, AJ 110, 2771]; (ii) 46 likely metal-weak thick disk stars within the range, $-2.20 \leq [\text{Fe}/\text{H}] \leq -1.00$ [Chiba, M., Beers, T.C., 2000, AJ 119, 2843]; (iii) 287 chemically selected G dwarfs within 25 pc from the Sun, with the corrections performed in order to take into account the stellar scale height [Rocha-Pinto, H.J., Maciel, W.J., 1996, MNRAS 279, 447]; in addition to previous results [Caimmi, R., 2001b, AN 322, 241; Caimmi, R., 2007, NewA 12, 289] related to (iv) 372 solar neighbourhood halo subdwarfs [Ryan, S.G., Norris, J.E., 1991, AJ 101, 1865]; and (v) 268 K-giant bulge stars [Sadler, E.M., Rich, R.M., Terndrup, D.M., 1996, AJ 112, 171]. The metal-poor and metal-rich EDMD related to the thick disk shows similarities with their halo and bulge counterparts, respectively. Then the thick disk is conceived as made of two distinct regions: the halo-like and the bulge-like thick disk, and the related EDMD is deduced. Under the assumption that each distribution is typical for the corresponding subsystem, the EDMD of the thick disk, the thick + thin disk, and the Galaxy, is determined by weighting the mass. In the second part, models of chemical evolution for the halo-like thick disk,

**Astronomy Department, Padua Univ., Vicolo Osservatorio 2, I-35122 Padova, Italy*
email: roberto.caimmi@unipd.it fax: 39-049-8278212

the bulge-like thick disk, and the thin disk, are computed assuming the instantaneous recycling approximation. The EDMD data are fitted, to an acceptable extent, by simple models of chemical evolution implying both homogeneous and inhomogeneous star formation, provided that star formation is inhibited during thick disk evolution, with respect to the thin disk. The initial mass function (IMF) is assumed to be a universal power law, which implies the same value of the true yield in different subsystems. The theoretical differential metallicity distribution (TDMD) is first determined for the halo-like thick disk, the bulge-like thick disk, and the thin disk separately, and then for the Galaxy by weighting the mass. An indicative comparison is performed between the EDMD deduced for the disk both in presence and in absence of [O/Fe] plateau, and its counterpart computed for (vi) $N = 523$ nearby stars within the range, $-1.5 < [\text{Fe}/\text{H}] < 0.5$, for which the oxygen abundance has been determined both in presence and in absence of the local thermodynamical equilibrium (LTE) approximation [Ramirez, I., Allende Prieto, C., Lambert, D.L., 2007, A&A 465, 271]. Both distributions are found to exhibit a similar trend, although systematic differences exist. In addition, the related empirical age-metallicity relation (EAMR) cannot be fitted by the theoretical age-metallicity relation (TAMR) predicted by the model, and the reasons for this discrepancy are explained.

keywords - galaxies: evolution - stars: formation; evolution.

1 Introduction

Abundance trends and the metallicity distribution within any Galactic subsystem are vital records to the formation and the evolution of the Milky Way. In particular, it can be wondered if each component underwent a separate chemical evolution both in space and in time, or some fraction of gas was transferred from an assigned reservoir into another one, implying violation of mass conservation. In the latter alternative, an additional question is if, and to what extent, simple models of chemical evolution can be used for each subsystem. To this respect, useful indications may be provided taking into consideration the G-dwarf problem.

In general, the occurrence of a G-dwarf problem is related to the observation of too few metal deficient G dwarfs (or of any other selected spectral class) with respect to that which could be expected from the Simple model of chemical evolution (e.g., Searle and Sargent, 1972; Pagel and Patchett, 1975; Haywood, 2001). It has been established in different regions of the Galaxy: the solar neighbourhood (van den Bergh, 1962; Schmidt, 1963) and,

to a lesser extent, the halo (e.g., Hartwick, 1976; Prantzos, 2003) and the bulge (e.g., Ferreras et al., 2003). In addition, a G-dwarf problem has been detected in both bulge-dominated and disk-dominated galaxies (Henry and Worthey, 1999), which is consistent with the idea that the G-dwarf problem is universal (Worthey et al., 1996).

The deficit of metal-poor stars (with respect to the prediction of the Simple model) may be interpreted in different ways, such as changes in the initial mass function (Schmidt, 1963; Adams and Fatuzzo, 1996; Bromm, 2004; Bromm and Larson, 2004; Larson, 2005), inflow of unprocessed (Larson, 1974; Lynden-Bell, 1975) or processed (Thacker et al., 2002) material from outside, evolution with inhomogeneous star formation (Searle, 1972; Malinie et al., 1993; Caimmi, 2000, 2001a, hereafter quoted together as C00¹; Caimmi, 2001b, hereafter quoted as C01; Oey, 2003; Karlsson, 2005; Caimmi, 2007, hereafter quoted as C07), instantaneous recycling approximation (Haywood, 2001), or overlooking the thick disk population (Haywood, 2006). For additional alternatives and further details refer to earlier attempts (Pagel and Patchett, 1975; Pagel, 1989).

Inhomogeneous (i.e. implying inhomogeneous star formation) models of chemical evolution succeed in both providing a solution to the G-dwarf problem and reproducing substantial scatter exhibited by the empirical age-metallicity relation (EAMR), with regard to the solar neighbourhood (e.g., Malinie et al., 1993; C00), halo stars (C01), and bulge stars (C07). The current paper aims to investigate if inhomogeneous simple models of chemical evolution are also consistent with the metallicity distribution in (i) the Galactic disk, conceived as made of three distinct subsystems: the metal-poor thick disk, the metal-rich thick disk, and the thin disk, and (ii) the Galaxy, conceived as made of five distinct subsystems: the above mentioned three, the halo, and the bulge. In any case, the related metallicity distribution is deduced (by weighting the mass) from the data belonging to selected samples (assumed to be representative of the whole subsystem).

Although the Galaxy is dominated (by mass and star number) by the two major subsystems, the bulge and the thin disk, still the contribution of the remaining ones, the halo and the thick disk, may be relevant in particular metallicity ranges. In addition, evidence for a halo-bulge and thick disk-thin disk collapse (Wyse and Gilmore, 1992; Ibata and Gilmore, 1995) implies that both the proto-halo and the proto-thick disk were more massive than their present counterparts. The empirical distribution of specific angular momen-

¹For this reference, two points may carefully be kept in mind, namely (i) values of a few parameters must be corrected as explained in Caimmi (2001b), Sect. 3, second paragraph, and (ii) the majority of figures do not correspond to the caption, as explained in the erratum (Caimmi, 2001a).

tum on the above mentioned subsystems, favours the idea of two different kinds of contraction (Wyse and Gilmore, 1992; Ibata and Gilmore, 1995). On the other hand, some evidence seems to exist on a continuous transition from an extended ($R \gtrsim 20$ kpc), pressure-supported halo, to an inner, flattened ($R \lesssim 15$ kpc), rotation-supported halo (Chiba and Beers, 2000). The chemical abundance of thick disk stars suggests a similar history to those of metal-rich ($[\text{Fe}/\text{H}] \approx -1.3$) halo stars, and the thick disk abundance patterns show excellent agreement with the chemical abundances observed in metal-poor bulge stars, suggesting the two populations were formed from the same reservoir at a common epoch (Prochaska et al., 2000).

The following samples have been taken as representative. For the thin disk, $N = 287$ chemically selected G dwarfs within 25 pc from the Sun, with the corrections performed in order to take into account the stellar scale heights (Rocha-Pinto and Maciel, 1996), hereafter quoted as the RM96 sample. For the halo, $N = 372$ kinematically selected subdwarfs (Ryan and Norris, 1991), hereafter quoted as the RN91 sample. For the bulge, $N = 268$ K-giants in Baade's window (Sadler et al., 1996), hereafter quoted as the SA96 sample. For the thick disk, a fictitious sample has been made from the following sources: (i) a normalized metallicity distribution (total number of stars not reported therein) related to a volume complete sample of local thick-disk stars, derived from Gliese and scaled in situ samples within the range, $-1.20 \leq [\text{Fe}/\text{H}] \leq -0.20$ (Wyse and Gilmore, 1995), hereafter quoted as the WG95 sample, and (ii) $N = 46$ likely metal-weak thick disk stars within the range, $-2.20 \leq [\text{Fe}/\text{H}] \leq -1.00$ (Chiba and Beers, 2000), hereafter quoted as the CB00 sample. Under the assumption that both WG95 and CB00 samples represent to an acceptable extent the related thick disk population, and keeping in mind that they overlap within the range, $-1.20 \leq [\text{Fe}/\text{H}] \leq -1.00$, a fictitious sample of $N = 592$ stars, hereafter quoted as the FS07 sample, can be derived for the thick disk.

The oxygen abundance is deduced from iron abundance, using two alternative relations involving the presence (PP) or absence (AP) of $[\text{O}/\text{Fe}]$ plateau for sufficiently low $[\text{Fe}/\text{H}]$ values (C01, C07). Though more precise dependences have been found in recent investigations (e.g., Jonsell et al., 2005; Fulbright et al., 2005; Garcia Perez et al., 2006; Melendez et al., 2006; Ramirez et al., 2007), related to different trends for different Galactic subsystems, still they are lying between the above mentioned alternatives, which shall be used to preserve comparison with earlier results (C01, C07).

The value of solar oxygen abundance also affects the $[\text{O}/\text{Fe}]-[\text{Fe}/\text{H}]$ relation. Recent determinations point towards lower values (e.g., Allende Prieto et al., 2001; Sofia and Meyer, 2001; Asplund et al., 2004; Melendez, 2004),

but the question is still under debate (e.g., Landi et al., 2007; Socas-Navarro and Norton, 2007). A solar oxygen mass abundance, $(Z_O)_\odot = 0.0056$, deduced from Allende-Prieto et al. (2001), shall be used to preserve comparison with earlier results (C01, C07).

Due to the above mentioned uncertainties, it has been preferred to deal with less recent EDMD determinations to preserve comparison with earlier work (C00; C01; C07). More recent, statistically more significant and less well scrutinised determinations e.g., the Geneva-Copenhagen survey (Nordstrom et al., 2004) for the local disk and the ongoing Hambourg survey performed by the Beers consortium (e.g., Prantzos, 2007) for the metal-poor halo, are related to iron abundance instead of oxygen abundance as in a selected sample of nearby stars (Ramirez et al., 2007), and for this reason shall not be used in the current attempt.

The empirical, differential metallicity distribution (EDMD), $\psi = \Delta N / (N\Delta\phi)$, $\log \phi = [\text{O}/\text{H}]$, has been determined in earlier attempts for the RN91 sample (C01) and the SA96 sample (C07), using both the PP and AP dependence of oxygen abundance on iron abundance. The same is done in Section 2 for the RM96 and the FS07 sample. In addition, a putative EDMD is derived for the thick + thin disk and the Galaxy, respectively, by weighting the mass of the related subsystems, in Section 3. A comparison with the predictions of simple models, involving homogeneous and inhomogeneous star formation, is given in Section 4 and 5, respectively. The discussion and the conclusion are the subject of Section 6 and 7, respectively.

2 The data

2.1 The empirical differential metallicity distribution

In dealing with simple models of chemical evolution, involving the assumption of instantaneous recycling, the predicted metal abundance has to be compared with the observed oxygen abundance (e.g., Pagel, 1989; C00; C01; C07). Unfortunately, oxygen is more difficult than iron to detect, and an empirical formula is needed, to express the former as a function of the latter.

On this matter a clear dichotomy appears between authors who support a plateau in $[\text{O}/\text{Fe}]$ for stars with $[\text{Fe}/\text{H}] \lesssim -1$ (e.g., Carretta et al., 2000); and those who do not (e.g., Israelian et al., 2001a, 2001b). Further insight can be gained by referring to specific proceedings (edited by Barbuy et al., 2001).

Taking the above alternatives as limiting situations, the following formu-

lae (C01; C07) shall be used:

$$\left[\frac{\text{O}}{\text{H}}\right] = \begin{cases} \left[\frac{\text{Fe}}{\text{H}}\right] + 0.6 ; & \left[\frac{\text{Fe}}{\text{H}}\right] \leq -1.2 ; & \left[\frac{\text{O}}{\text{H}}\right] \leq -0.6 ; \\ \frac{1}{2} \left[\frac{\text{Fe}}{\text{H}}\right] ; & \left[\frac{\text{Fe}}{\text{H}}\right] \geq -1.2 ; & \left[\frac{\text{O}}{\text{H}}\right] \geq -0.6 ; \end{cases} \quad (1)$$

$$\left[\frac{\text{O}}{\text{H}}\right] = \frac{2}{3} \left[\frac{\text{Fe}}{\text{H}}\right] ; \quad (2)$$

in presence or in absence of $[\text{Fe}/\text{H}]$ plateau, respectively. The value used for the oxygen solar abundance, $(Z_{\text{O}})_{\odot} = 0.0056 \mp 0.0006$, has been deduced from a number ratio, $\log(n_{\text{O}}/n_{\text{H}}) = -3.31 \mp 0.05$, or $A_{\text{O}} = \log(n_{\text{O}}/n_{\text{H}}) + 12 = 8.69 \mp 0.05$, corresponding to the solar photosphere line at 6300 Å (Allende-Prieto et al., 2001), assuming a hydrogen abundance, $X = 0.71$ (Anders and Grevesse, 1989). For further details refer to earlier work (C01). The assumed oxygen abundance agrees with recent results (e.g., Melendez, 2004; Asplund et al., 2004, 2005; Shchukina et al., 2005; Ramirez et al., 2007) in contrast with earlier determinations (e.g., Sauval et al., 1984; Grevesse et al., 1984; Anders and Grevesse, 1989) which yielded higher values ($A_{\text{O}} \approx 8.9$), but the question is still under debate (e.g., Landi et al., 2007; Socas-Navarro and Norton, 2007).

A number of $[\text{O}/\text{H}]-[\text{Fe}/\text{H}]$ dependences lying between those expressed by Eqs. (1) and (2), but different for different Galactic subsystems, have been derived from recent investigations (e.g., Bensby et al., 2004; Jonsell et al., 2005; Fulbright et al., 2005; Garcia Perez et al., 2006; Melendez et al., 2006; Ramirez et al., 2007). To allow comparison with previous results related to halo subdwarfs (C01) and K-giants in Baade’s window (C07), the solar oxygen abundance assumed therein (Allende Prieto et al., 2001) shall be used in the current attempt together with Eqs. (1) and (2), hereafter quoted as “in presence” and “in absence” of $[\text{O}/\text{Fe}]$ plateau, respectively, with regard to sufficiently low metallicities, $[\text{Fe}/\text{H}] \lesssim -1$.

Of course, the validity of Eqs. (1) and (2) shall be restricted to an epoch where only pop. II stars were present, $[\text{Fe}/\text{H}] < -4$ say, when the formation of extremely metal-deficient ($[\text{Fe}/\text{H}] < -4$) but oxygen overabundant (e.g., Christlieb et al., 2002; Bromm and Loeb, 2003; Iwamoto et al., 2005; Frebel et al., 2006) stars had already been occurred in presence of pop. III stars.

While observations are related to logarithmic number abundances, $[\text{A}/\text{H}] = \log(\text{A}/\text{H}) - \log(\text{A}/\text{H})_{\odot}$, models of chemical evolution deal with mass abundances, $Z_{\text{A}} = M_{\text{A}}/M$, where A is a generic element heavier than He, M_{A} is the total mass under the form of element, A, and M is the total mass under the form of any element. The following relation (Pagel, 1989; Malinie et al.,

1993; Rocha-Pinto and Maciel, 1996; C00; C01; C07):

$$\log \phi = \log \frac{Z_{\text{O}}}{(Z_{\text{O}})_{\odot}} = \left[\frac{\text{O}}{\text{H}} \right] ; \quad (3)$$

holds to a good extent². For a formal derivation refer to earlier work (C07, Appendix 1).

Let $\Delta \log \phi = \Delta[\text{O}/\text{H}] = [\text{O}/\text{H}]^+ - [\text{O}/\text{H}]^-$ be a logarithmic, oxygen abundance bin deduced from $\Delta[\text{Fe}/\text{H}]$ by use of Eq. (1) or (2). The related, oxygen abundance bin is:

$$\Delta \phi = \Delta^+ \phi + \Delta^- \phi ; \quad \Delta^{\mp} \phi = |\phi - \phi^{\mp}| ; \quad (4a)$$

$$\phi^{\mp} = \exp_{10} \left[\frac{\text{O}}{\text{H}} \right]^{\mp} ; \quad \phi = \frac{\phi^+ + \phi^-}{2} ; \quad (4b)$$

where in general, \exp_{ξ} defines the power of basis ξ and, in particular, \exp defines the power of basis e, according to the standard notation. To take also the RN91 sample into consideration, bins in $[\text{Fe}/\text{H}]$ equal to 0.2 dex shall be used (C01, C07).

Following earlier attempts (Pagel, 1989; Malinie et al., 1993; Rocha-Pinto and Maciel, 1996), the comparison between model predictions and observations shall be performed using the differential instead of the cumulative metallicity distribution, as it is a more sensitive test (Pagel, 1989) and allows direct comparison between different samples (Rocha-Pinto and Maciel, 1996). The occurrence of a sensitivity error in performing observations, precludes the use of a proper differential notation in dealing with the empirical differential metallicity distribution (hereafter referred to as EDMD³). This being the reason why the bin length cannot be lower than the sensitivity error, and differential ratios, i.e. first derivatives, $dN/d\phi$, must be replaced by increment ratios, $\Delta N/\Delta\phi$, where $\Delta\phi$ is the bin length, ΔN the number of sample objects within the selected bin, and N is the total number of sample objects.

Accordingly, the EDMD in a selected class of objects is defined as:

$$\psi(\phi \mp \Delta^{\mp} \phi) = \log \frac{\Delta N}{N \Delta \phi} ; \quad (5)$$

where the increment ratio, $\Delta N/\Delta\phi$, used in earlier attempts (Pagel, 1989; Malinie et al., 1993) has been replaced by its normalized counterpart, $\Delta N/$

²The oxygen mass abundance, Z_{O} , has been defined as O in C00 and C01, to simplify the notation therein.

³It is quoted as EGD in C00 and C01.

$(N\Delta\phi)$, used in more recent investigations (Rocha-Pinto and Maciel, 1996; C00; C01; C07), to allow comparison between different samples. The uncertainty on ΔN has been evaluated from Poisson errors (e.g., Ryan and Norris, 1991), as $\sigma_{\Delta N} = (\Delta N)^{1/2}$, and the related uncertainty in the EDMD is (e.g., C01; C07):

$$\Delta^{\mp}\psi = |\psi - \psi^{\mp}| = \log \left[1 \mp \frac{(\Delta N)^{1/2}}{\Delta N} \right] ; \quad (6a)$$

$$\psi^{\mp} = \log \frac{\Delta N \mp (\Delta N)^{1/2}}{N\Delta\phi} ; \quad (6b)$$

where $\psi^- \rightarrow -\infty$ in the limit $\Delta N \rightarrow 1$. For further details refer to earlier work (C01).

The $[\text{Fe}/\text{H}]$ - $[\text{O}/\text{H}]$ dependence and corresponding mean fractional oxygen abundance, ϕ , and half bin width, $\Delta^{\mp}\phi$, in presence of $[\text{O}/\text{Fe}]$ plateau (PP), according to Eq. (1), and in absence of $[\text{O}/\text{Fe}]$ plateau (AP), according to Eq. (2), respectively, are shown in Tab. 1 for the metallicity range of interest.

As in earlier attempts (Pagel, 1989; Malinie et al., 1993; Rocha-Pinto and Maciel, 1996; C00; C01; C07), the bin sizes in normalized oxygen abundance, ϕ , correspond to uniform bin sizes in $[\text{Fe}/\text{H}]$, according to Eqs. (3) and (4) and Tab. 1, which implies non uniform bin sizes, $\Delta\phi = 2\Delta^{\mp}\phi$, in the following tables and figures.

2.2 Metallicity distribution in the thick disk

Both the WG95 and CB00 samples are considered to infer the metallicity distribution in the thick disk. The total number of sample objects is not specified in the former case, as the related abundance distribution is normalized to unity (Wyse and Gilmore, 1995). A fictitious value, $N = 39$, is deduced from Tab. 3 therein, and shall be used in performing calculations. The metallicity range is $-1.20 \leq [\text{Fe}/\text{H}] \leq -0.20$ for the WG95 sample and $-2.20 \leq [\text{Fe}/\text{H}] \leq -1.00$ for the CB00 sample. The related EDMD, using Eqs. (3)-(6), is listed in Table 2 both in presence and in absence of $[\text{O}/\text{Fe}]$ plateau.

The samples under consideration overlap within the range, $-1.4 \leq [\text{Fe}/\text{H}] \leq -1.0$, which makes a renormalization be possible. The result is a fictitious sample: $N = 592$, and metallicity range, $-2.2 \leq [\text{Fe}/\text{H}] \leq -0.2$. The related EDMD is listed in Table 3 and plotted in Fig. 1 (top panels) both in presence and in absence of $[\text{O}/\text{Fe}]$ plateau. The trend exhibited looks like its counterpart related to the Galactic spheroid (C07). Having in mind it is

Table 1: The [Fe/H]-[O/H] dependence and corresponding mean fractional oxygen abundance, ϕ , and half bin width, $\Delta^\mp\phi$, in presence (PP) and in absence (AP) of [O/Fe] plateau.

		PP				AP			
[Fe/H] ⁻	[Fe/H] ⁺	3[O/H] ⁻	3[O/H] ⁺	ϕ	$\Delta^\mp\phi$	3[O/H] ⁻	3[O/H] ⁺	ϕ	$\Delta^\mp\phi$
1.2	1.4	1.8	2.1	4.496	0.515	2.4	2.8	7.443	1.134
1.0	1.2	1.5	1.8	3.572	0.409	2.0	2.4	5.476	0.834
0.8	1.0	1.2	1.5	2.837	0.325	1.6	2.0	4.028	0.613
0.6	0.8	0.9	1.2	2.254	0.258	1.2	1.6	2.963	0.451
0.4	0.6	0.6	0.9	1.790	0.205	0.8	1.2	2.180	0.332
0.2	0.4	0.3	0.6	1.422	0.163	0.4	0.8	1.604	0.244
0.0	0.2	0.0	0.3	1.129	0.129	0.0	0.4	1.180	0.180
-0.2	0.0	-0.3	0.0	0.897	0.103	-0.4	0.0	0.868	0.132
-0.4	-0.2	-0.6	-0.3	0.713	0.087	-0.8	-0.4	0.638	0.097
-0.6	-0.4	-0.9	-0.6	0.566	0.065	-1.2	-0.8	0.470	0.071
-0.8	-0.6	-1.2	-0.9	0.450	0.052	-1.6	-1.2	0.345	0.053
-1.0	-0.8	-1.5	-1.2	0.357	0.041	-2.0	-1.6	0.254	0.039
-1.2	-1.0	-1.8	-1.5	0.284	0.032	-2.4	-2.0	0.187	0.028
-1.4	-1.2	-2.4	-1.8	0.205	0.046	-2.8	-2.4	0.137	0.021
-1.6	-1.4	-3.0	-2.4	0.129	0.029	-3.2	-2.8	0.101	0.015
-1.8	-1.6	-3.6	-3.0	0.081	0.018	-3.6	-3.2	0.074	0.011
-2.0	-1.8	-4.2	-3.6	0.051	0.012	-4.0	-3.6	0.055	0.008
-2.2	-2.0	-4.8	-4.2	0.032	0.007	-4.4	-4.0	0.040	0.006
-2.4	-2.2	-5.4	-4.8	0.020	0.005	-4.8	-4.4	0.030	0.004
-2.6	-2.4	-6.0	-5.4	0.013	0.003	-5.2	-4.8	0.022	0.003
-2.8	-2.6	-6.6	-6.0	0.008	0.002	-5.6	-5.2	0.016	0.002
-3.0	-2.8	-7.2	-6.6	0.005	0.002	-6.0	-5.6	0.012	0.002
-3.7	-3.0	-9.3	-7.2	0.002	0.002	-7.4	-6.0	0.007	0.003

Table 2: The empirical, differential metallicity distribution (EDMD) in the thick disk, deduced from the CB00 sample ($N = 46$, top panel) and the WG95 sample ($N = 39$ deduced from a normalized distribution, bottom panel), both in presence (PP) and in absence (AP) of [O/Fe] plateau.

PP		AP		$\Delta^- \psi$	$\Delta^+ \psi$	ΔN
ϕ	ψ	ϕ	ψ			
0.284	0.810	0.187	0.868	0.113	0.090	19
0.205	0.328	0.137	0.668	0.176	0.125	9
0.129	0.051	0.101	0.337	0.374	0.198	3
0.081	0.480	0.074	0.694	0.257	0.161	5
0.051	0.656	0.055	0.832	0.257	0.161	5
0.032	0.890	0.040	0.957	0.257	0.161	5
0.713	0.013	0.638	-0.034	0.206	0.139	7
0.566	0.295	0.470	0.257	0.165	0.119	10
0.450	0.392	0.345	0.384	0.165	0.119	10
0.357	0.495	0.254	0.517	0.165	0.119	10
0.284	-0.397	0.187	-0.339	∞	0.301	1
0.205	-0.555	0.137	-0.214	∞	0.301	1

Table 3: The empirical, differential metallicity distribution (EDMD) in the thick disk, deduced from the FS07 sample ($N = 592$), both in presence (PP) and in absence (AP) of [O/Fe] plateau. Bottom and top panels correspond to halo-like and bulge-like thick disk, respectively. The related EDMD, calculated for the halo-like ($N = 18$) and the bulge-like ($N = 574$) thick disk subsample, is denoted as ψ_S .

PP			AP					
ϕ	ψ	ψ_S	ϕ	ψ	ψ_S	$\Delta^- \psi$	$\Delta^+ \psi$	ΔN
0.713	0.006	-0.008	0.638	-0.070	-0.056	0.046	0.042	98
0.566	0.261	0.273	0.470	0.218	0.235	0.038	0.035	140
0.450	0.361	0.370	0.345	0.352	0.362	0.038	0.035	140
0.357	0.461	0.473	0.254	0.485	0.495	0.038	0.035	140
0.284	-0.070	-0.047	0.187	-0.009	0.011	0.083	0.070	33
0.205	-0.378	-0.361	0.137	-0.033	-0.020	0.102	0.082	23
0.129	-1.062	0.458	0.101	-0.784	0.745	0.374	0.198	3
0.081	-0.640	0.887	0.074	-0.429	1.101	0.257	0.161	5
0.051	-0.440	1.063	0.055	-0.296	1.240	0.257	0.161	5
0.032	-0.240	1.298	0.040	-0.162	1.364	0.257	0.161	5

Table 4: The empirical, differential metallicity distribution (EDMD) in the thin disk, deduced from the RM96 sample ($N = 287$ and $N = 325.064$ after corrections due to stellar scale height; Rocha-Pinto and Maciel, 1996) both in presence (PP) and in absence (AP) of [O/Fe] plateau.

PP		AP				
ϕ	ψ	ϕ	ψ	$\Delta^- \psi$	$\Delta^+ \psi$	ΔN
1.422	-1.412	1.604	-1.587	0.295	0.174	4.110
1.129	-0.166	1.180	-0.309	0.061	0.054	57.410
0.897	0.136	0.868	0.027	0.048	0.043	91.490
0.713	0.225	0.638	0.149	0.049	0.044	89.127
0.566	0.004	0.470	-0.038	0.072	0.062	42.593
0.450	-0.064	0.345	-0.073	0.089	0.074	28.951
0.325	-0.614	0.226	-0.576	0.151	0.112	11.843

something else a mere coincidence, the fictitious FS07 sample is conceived as made of two fictitious subsamples related to different subsystems: a halo-like thick disk ($N = 18$) and a bulge-like thick disk ($N = 574$), in the metallicity range, $-2.2 \leq [\text{Fe}/\text{H}] \leq -1.4$ and $-1.4 \leq [\text{Fe}/\text{H}] \leq -0.2$, respectively. The corresponding EDMD is listed as ψ_S in Table 3 and plotted in Fig. 2, top and bottom panel, respectively, both in presence (left panels) and in absence (right panels) of [O/Fe] plateau.

The results from recent attempts involving a more refined abundance derivation (e.g., Reddy et al., 2006; Ramirez et al., 2007) are not used in the current paper, in absence (to the knowledge of the author) of their counterparts related to the halo, the bulge, and the metal-weak thick disk.

2.3 Metallicity distribution in the thin disk

As in an earlier attempt (C00), the RM96 sample ($N = 287$ and $N = 325.064$ after corrections due to stellar scale height; Rocha-Pinto and Maciel, 1996) is considered in the metallicity range, $-1.2 \leq [\text{Fe}/\text{H}] \leq 0.2$. The determination of the EDMD is repeated here owing to a different value of the assumed solar oxygen and, in addition, the absence of [O/Fe] plateau is considered.

The results, obtained by use of Eqs. (3)-(6), are listed in Table 4 both in presence and in absence of [O/Fe] plateau. The number of objects in each metallicity bin has been calculated as $\Delta N = \Delta N_0 / f + \delta(\Delta N)_1$, where ΔN_0 is the sample number, f and $\delta(\Delta N)_1$ are correction factors for the

stellar scale height and observational errors plus cosmic scatter, respectively (Rocha-Pinto and Maciel, 1996). Accordingly, the total number of objects reads $N = 325.064$. The related plots are shown in Fig. 1 (bottom panels) both in presence (left panels) and in absence (right panels) of [O/Fe] plateau. The dotted vertical line marks the transition from halo to bulge/disk globular cluster morphological type (Mackey and van den Bergh, 2005). For further details refer to earlier work (C07). The distribution could be bimodal with the occurrence of two maxima, related to low and intermediate oxygen abundance, respectively. The former maximum, if real, takes place near the transition from halo to bulge/disk globular cluster morphological type, as for old halo globular clusters and bulge K-giants in Baade’s window (C07).

Metallicity distributions with similar features are shown by other samples of thin disk stars (e.g., Wyse and Gilmore, 1995; Jørgensen, 2000; Kotoneva et al., 2002; Reddy et al., 2003). It has been questioned that the maximum of the distribution could be lowered by selection effects (Haywood, 2001). In fact, using different criteria, the maximum rises up to about the solar abundance (e.g., Favata et al., 1997; Haywood, 2001, 2006), but no general consensus seems still to exist on the selection of sample objects. For this reason, the RM96 sample shall be considered in the current paper.

3 Inferred metallicity distribution

Let the procedure used for the Galactic spheroid (C07) be generalized to a system made of n_S subsystems, where the EDMD related to a representative sample is available for each subsystem. The total mass is:

$$M = \sum_{i=1}^{n_S} M_i = \sum_{i=1}^{n_S} \frac{M_i}{M} M \quad ; \quad (7)$$

where M_i is the mass of i -th subsystem.

Let N be the total number of long-lived (i.e. life time longer than the age of the system) stars in the system, and ΔN the number of long-lived stars within a selected metallicity bin. The relative frequency, $\Delta N/N$, reads:

$$\frac{\Delta N}{N} = \sum_{i=1}^{n_S} \frac{\Delta N_i}{N} = \sum_{i=1}^{n_S} \frac{N_i}{N} \frac{\Delta N_i}{N_i} \quad ; \quad (8)$$

where ΔN_i and N_i are the number of long-lived stars within a selected metallicity bin and the total number, respectively, with regard to i -th subsystem. Then the relative frequency, $\Delta N/N$, related to the system, is expressed as a

mean of the relative frequencies, $\Delta N_i/N_i$, related to the subsystems, weighted by the factors, N_i/N .

Under the assumption of a universal initial mass function (IMF) for star generation, the number ratios, N_i/N , may safely be related to the mass ratios, M_i/M , as:

$$\frac{N_i}{N} = \frac{M_i}{M} ; \quad (9)$$

for further details refer to earlier work (C07).

The combination of Eqs. (8) and (9) yields:

$$\frac{\Delta N}{N} = \sum_{i=1}^{n_S} \frac{M_i}{M} \frac{\Delta N_i}{N_i} ; \quad (10)$$

where the relative frequencies, $\Delta N_i/N_i$, may be deduced from representative samples, which allows an evaluation of the relative frequency, $\Delta N/N$. The related uncertainty may be obtained using the standard formula of linear propagation of errors⁴ together with evaluation of Poisson errors (e.g., Ryan and Norris, 1991), $\sigma_{\Delta N_i} = (\Delta N_i)^{1/2}$. The result is:

$$\sigma_{\Delta N/N} = \sum_{i=1}^{n_S} \frac{M_i}{M} \frac{(\Delta N_i)^{1/2}}{N_i} ; \quad (11)$$

which may explicitly be calculated for assigned samples and mass ratios.

The EDMD related to the system results from the combination of Eqs. (5), (6), and (10), as:

$$\psi = \log \sum_{i=1}^{n_S} \frac{M_i}{M} \frac{\Delta N_i}{N_i \Delta \phi} ; \quad (12a)$$

$$\Delta^\mp \psi = \left| \log \left[1 \mp \frac{\sigma_{\Delta N/N}}{\Delta N/N} \right] \right| ; \quad (12b)$$

$$\psi^\mp = \log \sum_{i=1}^{n_S} \left[\frac{M_i}{M} \frac{\Delta N_i \mp (\Delta N_i)^{1/2}}{N_i \Delta \phi} \right] ; \quad (12c)$$

which may be particularized to the cases of interest.

3.1 The thick disk

The following assumptions have been made in Subsection 2.1 for deriving the halo-like and the bulge-like thick disk EDMD: (i) the parent samples WG95

⁴Linear propagation instead of quadratic propagation has been preferred to maximize the errors. The symbol, $\Delta(\Delta N)/N$, would be more germane to this respect, on the left-hand side of Eq. (11), but $\sigma_{\Delta N/N}$ is used to avoid confusion.

and CB00 represent to a comparable, acceptable extent the thick disk within the metallicity ranges, $-1.4 \leq [\text{Fe}/\text{H}] \leq -0.2$ and $-2.2 \leq [\text{Fe}/\text{H}] \leq -1.0$, respectively, to allow renormalization with respect to the common range, $-1.4 \leq [\text{Fe}/\text{H}] \leq -1.0$; (ii) objects belonging to the resulting FS07 sample, whose EDMD cannot be fitted by simple models of chemical evolution, come from different subsystems, whose EDMD can be fitted by simple models of chemical evolution, namely the halo-like ($[\text{Fe}/\text{H}] \leq -1.4$) and the bulge-like ($[\text{Fe}/\text{H}] > -1.4$) thick disk. In this view, the EDMD related to the thick disk depends, via Eqs. (12), on the halo-like to bulge-like thick disk mass ratio, $M_{\text{HK}}/M_{\text{BK}}$, which (to the knowledge of the author) is not available at present.

It has been suggested that the local density of the metal-weak thick disk population ($[\text{Fe}/\text{H}] \leq -1$) represents less than one percent of that of the canonical thick disk (Martin and Morrison, 1998) and, in any case, it appears to be a minor constituent of the entire thick disk population (Beers et al., 2002). It remains unclear whether the metal-weak thick disk population is properly considered an actual subsystem of the canonical thick disk with a distinct EDMD, or whether it corresponds, in reality, to the low-metal tail of the canonical thick disk EDMD (Beers et al., 2002). The former alternative has been chosen in the current attempt, according to the above considerations.

Different values of the mass ratio, $M_{\text{HK}}/M_{\text{BK}}$, make points related to halo-like and bulge-like thick disk (on the left and on the right, respectively, of the vertical dashed line in Fig. 1, top panels) EDMD shift vertically one with respect to the other: increasing values make the halo-like side of the distribution rise and the bulge-like side lower, and vice versa. The special case, $M_{\text{HK}}/M_{\text{BK}} = N_{\text{HK}}/N_{\text{BK}} = 18/574 \approx 0.03136$, leaves the thick disk EDMD (Fig. 1, top panels) unchanged, as plotted in Fig. 3 (top panels, crosses). The cases, $M_{\text{HK}}/M_{\text{BK}} = 0.01$ (triangles) and 0.10 (squares) are also represented for comparison, where the error bars are suppressed to avoid confusion.

3.2 The disk

The disk is conceived as made of three main subsystems, namely (i) the halo-like thick disk; (ii) the bulge-like thick disk; and (iii) the thin disk. Accordingly, the EDMD related to the disk depends, via Eqs. (12), on the halo-like to bulge-like thick disk mass ratio, $M_{\text{HK}}/M_{\text{BK}}$, and the thick to thin disk mass ratio, $M_{\text{KD}}/M_{\text{ND}}$, both unknown at present. The effect of the former ratio on the EDMD has been discussed in Subsection 3.1.

The cases, $M_{\text{KD}}/M_{\text{ND}} = 0.10, 0.05,$ and $0.20,$ are represented in Fig. 3 (bottom panels) as crosses, triangles, and squares, respectively, where the

error bars in the last two alternatives are suppressed to avoid confusion. In any case, $M_{\text{HK}}/M_{\text{BK}} = 18/574 \approx 0.03136$ has been adopted.

3.3 The Galaxy

The Galaxy is conceived as made of six main subsystems, namely: (i) globular clusters (GC); (ii) field halo stars (FH); (iii) field bulge stars (FB); (iv) field halo-like thick disk stars (HK); (v) field bulge-like thick disk stars (BK); and (vi) field thin disk stars (ND). As in C07, the following mass values are assumed:

$$M_{\text{GC}} = 0.001M_{10} \ ; \quad M_{\text{FH}} = 0.1M_{10} \ ; \quad M_{\text{FB}} = M_{10} \ ; \quad (13a)$$

$$M_{\text{KD}} = M_{\text{HK}} + M_{\text{BK}} \ ; \quad M_{\text{FD}} = M_{\text{KD}} + M_{\text{ND}} = 5.8M_{10} \ ; \quad (13b)$$

$$M_{\text{G}} = M_{\text{GC}} + M_{\text{FH}} + M_{\text{FB}} + M_{\text{FD}} = 6.901M_{10} \ ; \quad M_{10} = 10^{10}m_{\odot} \ ; (13c)$$

where the halo-like to bulge-like thick disk mass ratio, $M_{\text{HK}}/M_{\text{BK}}$, and the thick to thin disk mass ratio, $M_{\text{KD}}/M_{\text{ND}}$, remain undetermined and must be fixed.

The case, $M_{\text{HK}}/M_{\text{BK}} = 18/574 \approx 0.03136$ and $M_{\text{KD}}/M_{\text{ND}} = 0.1$, is represented in Fig. 4 (middle panels) and compared with its counterpart related to the Galactic spheroid (top panels, C07). Additional cases, $M_{\text{HK}}/M_{\text{BK}} = 0.01$ (triangles), 0.1 (squares), with $M_{\text{KD}}/M_{\text{ND}} = 0.1$; and $M_{\text{KD}}/M_{\text{ND}} = 0.05$ (diamonds), 0.2 (asterisks), with $M_{\text{HK}}/M_{\text{BK}} = 18/574$; are also presented in Fig. 4 (bottom panels). The related error bars are not shown to avoid confusion.

It is apparent that the effect of changing the halo-like to bulge-like thick disk mass ratio, $M_{\text{HK}}/M_{\text{BK}}$, and the thick to thin disk mass ratio, $M_{\text{KD}}/M_{\text{ND}}$, within reasonable ranges, yields an uncertainty on the EDMD which is of the same order as the Poisson error. Accordingly, from this point on the choice:

$$M_{\text{HK}}/M_{\text{BK}} = 18/574 \approx 0.03136 \ ; \quad M_{\text{KD}}/M_{\text{ND}} = 0.1 \ ; \quad (14)$$

shall be assumed as reference case.

The EDMD in the Galaxy looks like its counterpart related to the Galactic spheroid (halo + bulge), which is bimodal. It is apparent that (closed or open) simple models of chemical evolution cannot provide a satisfactory explanation to a bimodal EDMD, and a different model is needed (C07). In this view, let the main Galactic components i.e. the halo, the bulge, the thick disk, and the thin disk, be supposed to undergo distinct chemical evolutions. Let the thick disk be supposed to be substructured into two subsystems, the halo-like and the bulge-like thick disk which, in turn, undergo distinct chemical evolutions. The related theoretical differential metallicity distribution

(hereafter referred to as TDMD) is calculated in a selected spectral class of long-lived stars, and the resulting TDMD is compared with its empirical counterpart. To this aim, simple models implying both homogeneous and inhomogeneous star formation shall be used, as in earlier attempts (C01; C07).

4 Homogeneous simple models

Homogeneous simple models with (inhibiting star formation) gas (Hartwick, 1976) have widely been discussed in earlier attempts (C01; C07), and the interested reader is addressed therein for further details. What is relevant for the current paper, shall be reported in the following.

Homogeneous simple models of the kind considered imply four main assumptions, namely (i) instantaneous recycling; (ii) homogeneous star formation; (iii) universal power-law IMF; and (iv) gas inhibition from forming stars at a rate proportional to the star formation rate. Accordingly, the TDMD is represented as a straight line (e.g., Pagel, 1989; C00; C01; C07):

$$\psi(\phi) = \log \frac{dN}{N d\phi} = a\phi + b \quad ; \quad (15)$$

and the explicit expression of the coefficients, a and b , reads:

$$a = -\frac{1}{\ln 10} \frac{(Z_O)_\odot}{\hat{p}''} \quad ; \quad (16)$$

$$b = \log \left(\frac{\mu_o}{\mu_o - \mu_f} \frac{(Z_O)_\odot}{\hat{p}''} \right) - a\phi_o \quad ; \quad (17)$$

where $(Z_O)_\odot$ is the solar oxygen mass abundance, \hat{p}'' the effective (oxygen) yield, μ the (allowing star formation) gas mass fraction, and the indices, o and f , denote the beginning and the end of evolution, respectively.

The combination of Eqs. (16) and (17) yields, after some algebra:

$$\frac{\mu_f}{\mu_o} = 1 + \ln 10 \ a \exp_{10}(-a\phi_o - b) \quad ; \quad (18)$$

and the condition, $\mu_f/\mu_o \geq 0$, translates into:

$$b \geq -a\phi_o + \log(-\ln 10 \ a) \quad ; \quad (19)$$

which makes a restriction on (otherwise acceptable) linear fits to the EDMD.

The oxygen mass abundance, Z_O , to a large extent, may be related to the gas mass fraction, μ , as (e.g., Hartwick, 1976; Pagel, 1989; C00; C01; C07):

$$Z_O - (Z_O)_o = -\hat{p}'' \ln \frac{\mu}{\mu_o} ; \quad (20)$$

$$\hat{p}'' = \frac{\hat{p}}{1 + \kappa} ; \quad (21)$$

where \hat{p} , is the true (oxygen) yield and κ is the ratio of (inhibiting star formation) gas mass fraction to long-lived star and stellar remnant mass fraction.

It can be seen that a simple model with (inhibiting star formation) gas, lower mass limit of long-lived stars, m_{mf} , and inhibition parameter, κ , is equivalent to a simple model with the same values of independent parameters except the above mentioned two, $(m_{mf})_1 \leq m_{mf}$ and $\kappa_1 = 0 \leq \kappa$; and vice versa. Accordingly, the related (true) yield, \hat{p}_1 , has the same value as the effective yield, \hat{p}'' , expressed by Eq. (21). For further details refer to earlier papers (C01; C07).

For the models under consideration, the (inhibited from forming stars) gas mass fraction, D , is related to the long-lived star and stellar remnant mass fraction, s , as (e.g., Hartwick, 1976; C01; C07):

$$D(t) - D_o = \kappa[s(t) - s_o] ; \quad (22)$$

and mass conservation reads:

$$\mu(t) + s(t) + D(t) = 1 ; \quad (23)$$

where μ is the (allowing star formation) gas mass fraction. The combination of Eqs. (22) and (23) yields:

$$s - s_o = \frac{\mu_o - \mu}{1 + \kappa} ; \quad (24)$$

$$D - D_o = \frac{\kappa(\mu_o - \mu)}{1 + \kappa} ; \quad (25)$$

finally, the related EDMD can be determined following a standard procedure (e.g., Pagel and Patchett, 1975; Caimmi, 1981), as performed in C01.

With the aim of applying the above results to the chemical evolution of the Galaxy, the value of the true normalized yield, $\hat{p}/(Z_O)_\odot$, the long-lived star and stellar remnant mass fraction in a star generation, α , and the lower mass limit of long-lived stars, m_{mf} , shall be determined from a linear fit to the EDMD in the disk solar neighbourhood (C00) with regard to a solar

oxygen mass abundance, $(Z_{\text{O}})_{\odot} = 0.0056$ (C01), and inhibition parameter, $\kappa = 0$. Positive or negative values of κ , inferred from linear fits to the EDMD in a specified Galactic subsystem, would imply inhibited or enhanced star formation, respectively, in comparison to the disk solar neighbourhood.

Two extreme values of the power-law IMF exponent, p , shall be considered, namely: (i) $p = 2.9$, which is a fit to the IMF determined by Scalo (1986) or Miller and Scalo (1979), for $m \gtrsim m_{\odot}$ (Wang and Silk, 1993), and provides a good approximation also in terms of oxygen production (Wang and Silk, 1993), and (ii) $p = 2.35$, which coincides with the IMF determined by Salpeter (1955). More recent fits to the Scalo (1986) IMF yield a gentler slope, $p = 2.7$ (e.g., Weidner and Kroupa, 2005).

For fixed values of the normalized yield, \hat{p}/Z_{O} , and fractional oxygen abundance at the beginning and at the end of evolution, ϕ_o and ϕ_f , a change in the IMF slope leaves all the output parameters unaltered except the lower mass limit of long-lived stars, m_{mf} , the mass fraction of a star generation locked up in long-lived stars and stellar remnants, α , and the efficiency of star formation rate, C , where the product, αC , is also left unchanged (C01, Appendix C, Theorem 2). Accordingly, values of the above mentioned parameters, related to IMF exponents within the range, $2.35 < p < 2.9$, lie between their counterparts related to $p = 2.35$ and $p = 2.9$.

The characteristic stellar masses shall be taken as in earlier attempts (C00; C01; C07), namely: upper star mass limit, $\tilde{m}_{Mf} = 60$; neutron star progenitor lower mass limit, $\tilde{m}_{tr} = 9$; long-lived star upper mass limit, $\tilde{m}_{mr} = 1$; oxygen synthesising star lower mass limit, $\tilde{m}_{mrO} = 10.5$; typical neutron star mass, $\tilde{m}_{ns} = 1.5$; typical white dwarf mass, $\tilde{m}_{wd} = 0.6$; where $\tilde{m} = m/m_{\odot}$. For references see e.g.: \tilde{m}_{Mf} , \tilde{m}_{wd} (Wang and Silk, 1993); \tilde{m}_{ns} (Prantzos, 1994); \tilde{m}_{tr} (Prantzos and Silk, 1998); \tilde{m}_{mrO} (Pilyugin and Edmunds, 1996). On the other hand, the lower mass limit of long-lived stars, \tilde{m}_{mf} , results from the model.

Some parameters which remain fixed are listed in Tab. 5, where the indices, 2.9 and 2.35, denote the value of the power-law IMF exponent used in computing the corresponding quantities. The initial and final normalized oxygen abundance assumed for the halo-like thick disk, ϕ_{oH} and ϕ_{fH} , and the bulge-like thick disk, ϕ_{oB} and ϕ_{fB} , are $\phi_{oH} = 0.03$; $\phi_{fH} = \phi_{oB} = 0.16$; $\phi_{fB} = 0.80$. The thin disk shall not be considered, as a large fraction of the related EDMD cannot be fitted by homogeneous models (see Fig. 1, bottom panels).

For an assigned subsystem, different models can be obtained by changing a single remaining input parameter, chosen to be either the normalized effective yield, $\hat{p}''/(Z_{\text{O}})_{\odot}$, or the slope of the TDMD, a , which conforms to

Table 5: Values of parameters which remain fixed for different simple homogeneous models where star formation is inhibited. Star masses are normalized to the solar value, $\widetilde{m} = m/m_{\odot}$. The indices, 2.9 and 2.35, denote the value of the power-law IMF exponent used in computing the corresponding quantities.

$\hat{p}/(Z_{\text{O}})_{\odot} \cdot 10$	7.3722
$(\widetilde{m}_{mf})_{2.9} \cdot 10$	3.4235
$(\widetilde{m}_{mf})_{2.35} \cdot 10^3$	6.9136
$\alpha_{2.9} \cdot 10$	7.3666
$\alpha_{2.35} \cdot 10$	8.9104
$(Z_{\text{O}})_{\odot} \cdot 10^3$	5.6
μ_o	1
s_o	0
D_o	0

Eqs. (15) and (16). A few cases are listed in Tab. 6, related to the halo-like thick disk (HK) and the bulge-like thick disk (BK), respectively, where $\bar{\phi}$ represents the mean oxygen abundance (normalized to the solar value) of stars at the end of evolution. Model HK2 is very close to the limiting case, $\mu_f = 0$, defined by Eqs. (18) and (19). Values of parameters related to inhomogeneous simple models which fit the linear part of the EDMD in thin disk (DN), plotted in Fig. 1 (bottom panels), are listed for comparison.

It is apparent that halo-like and bulge-like thick disk models demand (to a different extent) inhibited star formation to maintain (i) universal power-law IMF, and (ii) true normalized yield, $\hat{p}/(Z_{\text{O}})_{\odot}$, unchanged with respect to a value deduced from an acceptable fit to the linear region of the EDMD in the thin disk solar neighbourhood (C00). More precisely, about 73-80% and 49-71% of the initial halo-like and bulge-like thick disk gas, respectively, has to be inhibited from forming stars, for providing an acceptable fit to the related EDMD. It results in a normalized effective yield, $\hat{p}''/(Z_{\text{O}})_{\odot}$, about three-four times lower in the halo-like thick disk with respect to the bulge-like thick disk. It is worth remembering that the above difference raises to about one order of magnitude for the halo and the bulge, and enhanced (instead of inhibited) star formation is demanded for the latter. For further details refer to earlier work (C07).

The TDMD deduced from models HK1-HK2 and BK1-BK2 is represented in Fig. 5 and compared to the corresponding EDMD in connection with halo-

Table 6: Values of parameters related to homogeneous simple models where star formation is inhibited, corresponding to linear fits to the empirical differential metallicity distribution (EDMD) in halo-like (HK) and bulge-like (BK) thick disk, plotted in Fig. 2. The mean oxygen abundance (normalized to the solar value) of stars at the end of evolution is denoted as $\bar{\phi}$. Model HK2 is very close to the limiting case, $\mu_f = 0$, defined by Eqs. (18) and (19). Values of parameters related to inhomogeneous simple models which fit the linear part of the EDMD in thin disk (DN), plotted in Fig. 1 (bottom panels), are listed for comparison. The definition, $Y = \hat{p}''/(Z_O)_\odot$, is to save space.

	HK1	HK2	BK1	BK2	DN1	DN2
Y	8.3518 E-2	6.8285 E-2	3.6191 E-1	2.0508 E-1	4.4233 E-1	4.4233 E-1
$-a$	5.2000 E-0	6.3600 E-0	1.2000 E-0	2.1176 E-0	9.8183 E-1	9.8183 E-1
b	1.3170 E-0	1.3885 E-0	8.1340 E-1	1.3311 E-0	1.0210 E-0	9.7643 E-1
κ	7.8271 E-0	9.7962 E-0	1.0370 E-0	2.5947 E-0	0.0000 E-0	0.0000 E-0
μ_f	1.7355 E-1	7.1092 E-2	2.7260 E-2	1.7656 E-2	2.9047 E-1	1.2799 E-1
s_f	9.3627 E-2	8.6040 E-2	4.7753 E-1	2.7327 E-1	7.0953 E-1	8.7201 E-1
D_f	7.3283 E-1	8.4287 E-1	4.9521 E-1	7.0907 E-1	0.0000 E-0	0.0000 E-0
$\bar{\phi}$	8.2804 E-2	8.4469 E-2	6.2538 E-1	4.9020 E-1	5.9389 E-1	5.0003 E-1

like thick disk (top panels), bulge-like thick disk (middle panels), and thin disk (bottom panels) stars, both in presence (left panels) and in absence (right panels) of [O/Fe] plateau.

Though the linear fit to the thin disk EDMD is derived using inhomogeneous models (C00), still it can be related to homogeneous models where $a = -0.98183$; $\hat{p}''/(Z_{\odot})_{\odot} = 0.44233$; and $b = 1.0211$ (PP), $b = 0.97643$ (AP). The dashed line in top panels corresponds to model HK2 in Table 6, which is very close to the limiting case, $\mu_f = 0$, defined by Eqs. (18) and (19), and model HK1 is represented by the less inclined (in absolute value) full line. Accordingly, the linear fits lying between the dashed line and the more inclined (in absolute value) full line, must be excluded.

For the halo-like thick disk, homogeneous simple models in the presence of inhibited star formation provide an acceptable fit (though in a restricted range) with values of input parameters as listed in Tab. 5 and $\phi_{oH} = 0.03$; $\phi_{fH} = 0.16$; $0.068 < \hat{p}''/(Z_{\odot})_{\odot} < 0.084$, both in presence and in absence of [O/Fe] plateau.

For the bulge-like thick disk, homogeneous simple models in the presence of inhibited star formation provide an acceptable fit with values of input parameters as listed in Tab. 5 and $\phi_{oB} = 0.16$; $\phi_{fB} = 0.80$; $0.205 < \hat{p}''/(Z_{\odot})_{\odot} < 0.362$, both in presence and in absence of [O/Fe] plateau.

For the thin disk (represented for comparison), homogeneous simple models provide no acceptable fit with values of input parameters as listed in Tab. 5 and $\phi_{oN} = 0.325$, $\phi_{fN} = 1.58$, (PP); $\phi_{oN} = 0.226$, $\phi_{fN} = 1.85$, (AP); $\hat{p}''/(Z_{\odot})_{\odot} = \hat{p}/(Z_{\odot})_{\odot} = 0.44233$.

Further inspection of Fig. 5 shows a marked deficiency in the number of stars observed below a threshold, $[\text{Fe}/\text{H}] \approx -1$ for the bulge-like thick disk and $[\text{Fe}/\text{H}] \approx -0.8$ for the thin disk, which is close to the transition from halo to bulge/disk globular cluster morphological type. In other words, a G-dwarf problem seems to exist for both the bulge-like thick disk and the thin disk.

Let dN_i be the predicted total number of long-lived stars within the i -th subsystem ($1 \leq i \leq n_S$) belonging to a system, related to a fractional oxygen metal abundance, $\phi \mp d\phi/2$, with regard to a simple homogeneous model of chemical evolution. Let N_i be the predicted total number of long-lived stars within the above mentioned subsystem. The predicted counterparts for the whole system, related to the selected models, are $dN = \sum_i dN_i$ and $N = \sum_i N_i$, respectively.

The relative frequency, dN/N , reads:

$$\frac{dN}{N} = \sum_{i=1}^{n_S} \frac{dN_i}{N} = \sum_{i=1}^{n_S} \frac{N_i}{N} \frac{dN_i}{N_i} ; \quad (26)$$

or, using Eq. (9):

$$\frac{dN}{N} = \sum_{i=1}^{n_S} \frac{M_i}{M} \frac{dN_i}{N_i} ; \quad (27)$$

where M_i and M are the mass of the subsystem and the whole system, respectively.

The TDMD related to the whole system, keeping in mind Eq. (15), is:

$$\psi = \log \frac{dN}{N d\phi} = \log \sum_{i=1}^{n_S} \frac{dN_i}{N d\phi} = \log \sum_{i=1}^{n_S} \frac{N_i}{N} \frac{dN_i}{N_i d\phi} ; \quad (28)$$

and the combination of Eqs. (9), (15), and (28) yields:

$$\psi = \log \sum_{i=1}^{n_S} \frac{M_i}{M} \exp_{10}(a_i \phi + b_i) ; \quad (29)$$

where the particularization to the thick disk, the thick + thin disk, and the Galaxy, is defined by Eqs. (13) and (14).

Two alternatives shall be considered, K_1 and K_2 (halo-like + bulge-like thick disk), D_1 and D_2 (thick + thin disk), G_1 and G_2 (Galaxy), according if the coefficients, a_i and b_i , are taken from cases HK1, BK1, or HK2, BK2, of Table 6; DN1 or DN2 of Table 6; H1, B1, or H2, B2, of Table 8 (C07), respectively. The last models are related to the halo (H) and bulge (B), which are needed in dealing with the Galaxy.

The TDMD related to the halo-like + bulge-like thick disk and to the thick + thin disk, is plotted in Fig. 6 (top and bottom panels, respectively) and compared to its empirical counterpart, represented in Fig. 3 (crosses), both in presence (left panels) and in absence (right panels) of [O/Fe] plateau. A discontinuity is exhibited by the TDMD, where bulge-like thick disk or thin disk formation is assumed to start.

The TDMD related to the Galaxy is plotted in Fig. 7 and compared to its empirical counterpart represented in Fig. 4 (middle panels), both in presence (left panels) and in absence (right panels) of [O/Fe] plateau. Discontinuities are exhibited by the TDMD where bulge, halo-like thick disk, bulge-like thick disk, and thin disk formation are assumed to start.

Although a G-dwarf problem seems to exist for both the halo, the bulge, the halo-like thick disk, the bulge-like thick disk, and the thin disk, the current model provides a viable interpretation to the occurrence of three extremum points, two maxima and one minimum, in the EDMD.

5 Inhomogeneous, simple models

Inhomogeneous simple models with (inhibiting star formation) gas have widely been discussed in earlier attempts (C01; C07), following the basic formulation of the model (Malinie et al., 1993; C00), and the interested reader is addressed therein for further details. What is relevant for the current paper, shall be reported in the following.

In the light of the model, each Galactic subsystem is conceived as being structured into a number of discrete, entirely gaseous, identical regions, and a background of long-lived stars, stellar remnants, and gas inhibited from star formation, which have been generated earlier. The evolution occurs via a sequence of identical time steps. At the beginning of each step, star formation stochastically takes place in a subclass of “active” regions, as described by simple homogeneous models, while the others remain “quiescent”. At the end of each step, high-mass stars have died whereas low-mass stars have survived up until today, according to instantaneous recycling approximation. In addition, the enriched gas which remains from active regions is instantaneously mixed with the unenriched gas within quiescent regions, to form a new set of identical regions for the next step.

To allow comparison between simple homogeneous and inhomogeneous models, the current investigation shall be restricted to the special case of expected evolution, where the fraction of active regions is time-independent. With respect to the general case, both the theoretical age-metallicity relation (TAMR) and the TDMD exhibit minor changes for the disk solar neighbourhood (C00) and negligible variations for the halo solar neighbourhood (C01).

In any case, active regions evolve as in the Hartwick’s (1976) model, yielding the usual relationship between the newly synthesised oxygen gas mass fraction within an active region, $\Delta^*(Z'_O)_R$, and the gas mass fraction within an active region, μ'_R , at the end of each step in the following way:

$$\Delta^*(Z'_O)_R = -\hat{p}'' \ln(\mu'_R) \quad ; \quad (30)$$

provided that the IMF is universal and the effects of initial composition on star evolution are neglected.

The newly synthesised oxygen gas mass fraction, due to an active region, within the system, $\Delta^*(Z_O)_R$, at the end of each step, is (C00):

$$\Delta^*(Z_O)_R = \frac{\mu'_R}{n[1 - \chi(1 - \mu'_R)]} \Delta^*(Z'_O)_R \quad ; \quad (31)$$

where n is the number of active and quiescent regions, χ the probability of a region being active, and both remain constant during the expected evolution.

The newly synthesised oxygen gas mass fraction, due to all active regions, within the system, $\Delta^* Z_{\text{O}}$, at the end of each step, is (C00):

$$\Delta^* Z_{\text{O}} = k \Delta^*(Z_{\text{O}})_{\text{R}} = n \chi \Delta^*(Z_{\text{O}})_{\text{R}} \quad ; \quad (32)$$

where $k = n \chi$ is the number of active regions.

The changes in (allowing star formation) gas and oxygen abundance, related to the $(\ell + 1)$ -th step, read (C00; C01):

$$\mu_{\ell+1} = \mu_{\ell} q = \mu_o q^{\ell+1} \quad ; \quad (33)$$

$$(Z_{\text{O}})_{\ell+1} = (Z_{\text{O}})_{\ell} + \Delta^* Z_{\text{O}} = (Z_{\text{O}})_o + (\ell + 1) \Delta^* Z_{\text{O}} \quad ; \quad (34)$$

$$\Delta^* Z_{\text{O}} = - \frac{\hat{p}'' (1 - q) \mu'_{\text{R}} \ln(\mu'_{\text{R}})}{(1 - \mu'_{\text{R}}) q} \quad ; \quad (35)$$

$$q = 1 - \chi (1 - \mu'_{\text{R}}) \quad ; \quad 0 \leq q \leq 1 \quad ; \quad (36)$$

where the parameter, q , may be considered as an effective gas mass fraction within a region at the end of each step, i.e. the mean gas mass fraction averaged on both active and quiescent regions.

The combination of Eqs. (30)-(36) yields:

$$(Z_{\text{O}})_{\ell+1} = (Z_{\text{O}})_o - \hat{p}' [\ln(\mu_{\ell+1}) - \ln(\mu_o)] \quad ; \quad (37)$$

$$\Delta^* Z_{\text{O}} = -\hat{p}' \ln q \quad ; \quad (38)$$

$$\hat{p}' = \hat{p}'' \frac{(1 - q) \mu'_{\text{R}} \ln \mu'_{\text{R}}}{(1 - \mu'_{\text{R}}) q \ln q} \quad ; \quad \hat{p}' \leq \hat{p}'' \quad ; \quad (39)$$

where \hat{p}' is an effective yield due to both inhomogeneous star formation and inhibited star formation. In the limit of instantaneous recycling i.e. chemically homogeneous interstellar medium (e.g., the Simple model, Hartwick's model), $\chi \rightarrow 1$, $q \rightarrow \mu'_{\text{R}}$, and $\hat{p}' \rightarrow \hat{p}''$.

According to Eq. (37), the dependence of oxygen abundance on the gas mass fraction in inhomogeneous models remains unchanged with respect to homogeneous models provided that: (i) the expected evolution is considered; (ii) the probability of a region being active, χ_{ℓ} , the gas mass fraction within a region, $\mu'_{\text{R}\ell}$, and the (true) yield, \hat{p}_{ℓ} , during the $(\ell + 1)$ -th step, do not depend on the evolution; and (iii) the effective yield, \hat{p}'_{ℓ} , is replaced by the effective yield, \hat{p}_{ℓ} . In absence of inhibited star formation, it can be shown that the effective yield, \hat{p}' , takes the same expression as in the inhomogeneous model of Malinie et al. (1993). For further details refer to earlier papers (C00, C01).

Although the TDMD cannot be analytically expressed in the framework of inhomogeneous simple models, it still can in the special case of expected

evolution, with regard to the starting point, $\psi(\phi_o) = \psi_o$, and the ending point of the initial step, $\psi(\phi_o + \Delta^*\phi_o) = \psi_1$, where $\Delta^*\phi_o$ is the net oxygen abundance (normalized to the solar value) increase in gas component at the end of the first step. The related explicit expressions can be found in previous work [C01; C07, Eqs. (39) and (40) therein]. An approximate expression of the TDMD related to the first step, ψ_1 , with the terms up to the second order retained, can be found in previous work [C01; C07, Eq. (41) therein]. The last expression is valid also in the general case, provided $\Delta^*\phi$ is replaced by $\Delta^*\phi_o$ and the probability, χ , by the relative frequency, $\nu_o = k_o/n_o$, being k_o and n_o the number of active and all regions, respectively, with regard to the first step.

The values of some parameters related to the expected evolution, concerning cases HK1, HK2; BK1, BK2; DN1, DN2; are listed in Table 7.

The parameters appearing therein, which equal their counterparts corresponding to homogeneous models (Tables 5 and 6, cases HK and BK), must be connected with active regions, and for this reason some corresponding output parameters show different values. For further details refer to earlier work (C07, Appendix B). It is worth recalling that cases DN1 and DN2 listed in Table 6 for comparison, are related to inhomogeneous models listed in Table 7.

New input parameters are: the effective yield, \hat{p}' , and the normalized oxygen abundance increase at the end of a step with regard to the whole system, $\Delta^*\phi$, and to an active region, $\Delta^*\phi'_R$, respectively. In presence of inhibited (from forming stars) gas (cases HK and BK), the star and inhibited gas mass fraction related to the whole system at the end of evolution, s_f and D_f , are expressed in terms of their counterparts related to an active region at the end of a step, s'_R and D'_R , as (C07):

$$s_f = \frac{1 - \mu_f}{1 - \mu'_R} s'_R ; \quad (40)$$

$$D_f = \frac{1 - \mu_f}{1 - \mu'_R} D'_R ; \quad (41)$$

which are listed in the lower part of Tab. 7. For further details refer to earlier work (C07).

The TDMD related to cases HK1, BK1, DN1, (full lines) and HK2, BK2, DN2, (dashed lines) is compared in Fig. 8 to the corresponding EDMD with regard to halo-like thick disk (top panels), bulge-like thick disk (middle panels), and thin disk (bottom panels) stars, both in presence (left panels) and in absence (right panels) of [O/Fe] plateau.

Inhomogeneous simple models with inhibited star formation provide an acceptable fit using values of input parameters listed in Table 5 and $0.031 <$

Table 7: Values of parameters related to the expected evolution of inhomogeneous simple models, in connection with two different cases for the halo-like thick disk, HK1 and HK2, for the bulge-like thick disk, BK1 and BK2, and for the thin disk, DN1 and DN2, respectively. The indices, 2.9 and 2.35, denote values related to the power-law IMF exponent, p , in computing the corresponding quantities. For the parameter, ψ_1 , upper and lower values are calculated as in C07 by use of Eqs. (40) and (41) therein, respectively. The effective yield, \hat{p}' , is related to inhomogeneities in oxygen abundance due to the presence of active and quiescent regions, whereas oxygen is uniformly distributed within active regions. The lower part of the table (last 6 rows) is related to models with inhibited star formation. Parameters not reported therein have the same value as in the upper part, with the exception of \hat{p} , α , and m_{mf} , which are listed in Tab.5 together with other parameters not appearing here. The effective yield, \hat{p}'' , due to the presence of (inhibiting star formation) gas within active regions, is listed as \hat{p} in the upper part of the table. The effective yield, \hat{p}' , due to the presence of both (inhibiting star formation) gas within active regions, and (precluding star formation) gas within quiescent regions, is listed with the same notation in the upper part of the table. The index, R, denotes a generic active region. The mean oxygen abundance (normalized to the solar value) of stars at the end of evolution is denoted as $\bar{\phi}$.

	HK1	HK2	BK1	BK2	DN1	DN2
μ'_R	2.3356 E-1	2.0512 E-1	2.1579 E-1	1.2933 E-1	3.7148 E-1	3.6106 E-1
q	9.2861 E-1	7.9327 E-1	8.4346 E-1	4.5877 E-1	9.5175 E-1	9.2106 E-1
χ	9.3147 E-2	2.6007 E-1	1.9961 E-1	6.2162 E-1	7.6765 E-2	1.2355 E-1
$\hat{p}/(Z_O)_\odot$	8.3518 E-2	6.8285 E-2	3.6191 E-1	2.0508 E-1	7.3722 E-1	7.3722 E-1
$\hat{p}'/(Z_O)_\odot$	3.8418 E-2	3.1411 E-2	1.6648 E-1	9.4338 E-2	4.4233 E-1	4.4233 E-1
μ_f	7.4358 E-1	3.9599 E-1	5.0613 E-1	4.4298 E-2	2.9047 E-1	1.2799 E-1
$\alpha_{2.9}$	9.6108 E-1	9.6795 E-1	8.5071 E-1	9.0955 E-1	7.3666 E-1	7.3666 E-1
$\alpha_{2.35}$	9.8634 E-1	9.8880 E-1	9.4337 E-1	9.6710 E-1	8.9104 E-1	8.9104 E-1
$(\widetilde{m}_{mf})_{2.9}$	4.1289 E-2	3.3283 E-2	1.8306 E-1	1.0516 E-1	3.4235 E-1	3.4235 E-1
$(\widetilde{m}_{mf})_{2.35}$	2.0404 E-5	1.1592 E-5	1.1294 E-3	2.4576 E-4	6.9136 E-3	6.9136 E-3
$\Delta^* \phi$	2.8456 E-3	7.2745 E-3	2.8341 E-2	7.3509 E-2	2.1874 E-2	3.6375 E-2
$\Delta^* \phi'_R$	1.2146 E-1	1.0818 E-1	5.5498 E-1	4.1947 E-1	7.3003 E-1	7.5101 E-1
ψ_o	6.3844 E-1	7.9973 E-1	4.7970 E-2	5.0128 E-1	-8.3341 E-1	-7.1627 E-1
$\psi_1(40)$	6.3107 E-1	7.7680 E-1	3.1076 E-2	4.2576 E-1	-8.3984 E-1	-7.2694 E-1
$\psi_1(41)$	6.3104 E-1	7.7659 E-1	3.0965 E-2	4.2344 E-1	-8.3985 E-1	-7.2698 E-1
κ	7.8271 E-0	9.7962 E-0	1.0370 E-0	2.5947 E-0	0.0000 E-0	0.0000 E-0
s'_R	8.6829 E-2	7.3626 E-2	3.8498 E-1	2.4221 E-1	6.2852 E-1	6.3894 E-1
D'_R	6.7962 E-1	7.2126 E-1	3.9923 E-1	6.2846 E-1	0.0000 E-0	0.0000 E-0
$\bar{\phi}$	7.6505 E-2	7.0371 E-2	3.6920 E-1	3.0277 E-1	5.9389 E-1	5.0003 E-1
s_f	2.9049 E-2	5.5946 E-2	2.4245 E-1	2.6586 E-1	7.0953 E-1	8.7201 E-1
D_f	2.2737 E-1	5.4806 E-1	2.5142 E-1	6.8984 E-1	0.0000 E-0	0.0000 E-0

$\hat{p}'/(Z_{\text{O}})_{\odot} < 0.039$ (halo-like thick disk); $0.094 < \hat{p}'/(Z_{\text{O}})_{\odot} < 0.167$ (bulge-like thick disk); in and $\hat{p}'/(Z_{\text{O}})_{\odot} \approx 0.442$ (thin disk).

In dealing with active regions, the normalized oxygen abundance at the end of evolution, ϕ_f , has to be replaced with the normalized oxygen abundance at the end of a step, $\phi_i + \Delta^* \phi'_{\text{R}}$.

Further inspection of Fig. 8 shows that, with respect to homogeneous simple models plotted in Fig. 5, the fit is more or less unchanged for the halo-like thick disk, slightly worsened for the bulge-like thick disk in presence of [O/Fe] plateau, but substantially improved for the bulge-like thick disk in absence of [O/Fe] plateau and the thin disk. In addition, a G-dwarf problem still remains (but alleviated) only for the bulge-like thick disk in presence of [O/Fe] plateau.

The TDMD related to a system made of different subsystems, has to be numerically computed using Eqs. (13) and (28) for assigned values of the thick disk to thin disk mass ratio, $M_{\text{KD}}/M_{\text{ND}}$, and halo-like to bulge-like thick disk mass ratio, $M_{\text{HK}}/M_{\text{BK}}$. The following models have been considered with regard to the reference case: K1 and K2 for the thick disk, using models HK1, BK1, and HK2, BK2, respectively, defined in Table 7; D1 and D2 for the thick + thin disk, using models HK1, BK1, DN1, and HK2, BK2, DN2, respectively, defined in Table 7. A comparison with the related EDMD (Fig. 3, top and bottom panels, respectively, crosses) is made in Fig. 9 (top and bottom panels, respectively) both in presence (left panels) and in absence (right panels) of [O/Fe] plateau. The trend looks like its counterpart exhibited by homogeneous simple models (Fig. 6) but the fit is improved, and similar considerations can be made.

The following models have also been considered: G1 and G2 for the Galaxy, using models H1, B1, HK1, BK1, DN1, and H2, B2, HK2, BK2, DN2, respectively, where models H and B are related to the halo and the bulge, respectively, and are defined in C07 (Table 9). A comparison with the related EDMD (Fig. 4, middle and bottom panels, crosses) is made in Fig. 10 both in presence (left panels) and in absence (right panels) of [O/Fe] plateau. The trend looks like its counterpart exhibited by homogeneous simple models (Fig. 7) but the fit is improved, and similar considerations can be made.

In the framework of inhomogeneous models, both active and quiescent regins must take origin from (allowing star formation) gas. An inspection of Table 7 shows that, for models HK, only a few percent (2.9-5.6%) of the total mass has been converted into (long-lived) stars, leaving about 74-39% in (allowing star formation) gas; and about 22-55% in (inhibiting star formation) gas; for models BK, about one quarter (24-27%) of the total mass has been converted into (long-lived) stars, leaving about 51-4% in (allowing star formation) gas; and about 29-69% in (inhibiting star formation) gas; for models

DN, more than two thirds (71-87%) of the total mass has been converted into (long-lived) stars, leaving about 29-13% in (allowing star formation) gas; and no (inhibiting star formation) gas.

The mean normalized oxygen abundance within long-lived stars is $\bar{\phi} = 0.077$ - 0.070 , 0.37 - 0.30 , and 0.60 - 0.50 , in the halo-like thick disk, the bulge-like thick disk, and the thin disk, respectively.

It is worth noting that the Galaxy would be mostly luminous for a IMF exponent, $p = 2.9$, and lower stellar mass limit, $\tilde{m}_{\text{mf}} \approx 0.34$, and mostly dark for $p = 2.35$ and $\tilde{m}_{\text{mf}} \approx 0.007$. On the other hand, the assumption of an universal IMF implies the same value of the true yield and lower mass limit of long-lived stars, for Galactic subsystems.

6 Discussion

Although the Galaxy appears to be dominated (by mass and star number) by the two major subsystems, the bulge and the thin disk, still the contrary holds with respect to selected metallicity bins. For instance, low-metallicity bins are dominated by halo stars. Even if the spheroid and the disk evolved separately (albeit with similar present metal abundance), the distribution of specific angular momentum is known to be consistent with both a halo-bulge and a thick disk-thin disk (Wyse and Gilmore, 1992; Ibata and Gilmore, 1995) collapse. Then in early times a reversed situation occurred, where the main Galactic components were the halo and the thick disk, and gas exchange between the two reservoirs cannot be excluded. Some signature of the formation and the early evolution of the Galaxy could be found in the EDMD related to the whole system. In this view, the thick disk has to be conceived as pre-existing with respect to the thin disk. For a discussion of different scenarios on the origin of the thick disk see e.g., Gilmore et al. (1995).

In brief, the method used in the current and earlier work (C07) is the following. An assigned system (e.g., the Galactic spheroid, the Galactic thick disk, the Galactic disk, the Galaxy) is conceived as made of a number of subsystems where the chemical evolution occurs separately. Then the resulting EDMD and TDMD are calculated using Eqs. (9), (15), and (28), i.e. weighting by mass. The larger uncertainty concerns the thick disk, where (i) two different samples (WG95 and CB00) have been renormalized under the assumption that they are equally representative of objects belonging to the metallicity range in common, and (ii) the resulting sample (FS07), has been conceived as made of two different kind of objects, belonging to the halo-like or the bulge-like thick disk, according if the related low-metallicity

and the high-metallicity EDMD resembles its halo and bulge counterpart, respectively. In this view, the results are merely indicative and need to be confirmed using more complete samples. In any case, the G-dwarf problem in the bulge-like thick disk, the thick + thin disk, and the Galaxy, is alleviated for homogeneous models and much strongly for inhomogeneous models, with respect to models where chemical evolution occurs at the same extent in different subsystems.

The absence of a G-dwarf problem in the (thick + thin) Galactic disk has been established in a recent attempt (Haywood, 2006), using the Simple model. It is not in contradiction with the results of the current paper, for the following reasons. First, scalelength corrections in thin disk samples have been used in Haywood (2006), while different samples belonging to the thick and the thin disk have been used in the current paper. Second, the chemical evolution has been assumed to occur at the same rate in the whole disk in Haywood (2006), while a different extent has been considered in the current paper, according if the halo-like thick disk, the bulge-like thick disk, and the thin disk, are dealt with.

A lower mass limit of long-lived stars, exceeding the theoretical Jeans stellar mass ($0.007 \leq \tilde{m}_J \leq 0.01$), occurs for a power-law exponent $p = 2.9$, which is a fit to the Scalo (1986) IMF for $m \gtrsim m_\odot$, concerning both mass distribution and oxygen production (Wang and Silk, 1993). A less steep Salpeter (1955) IMF, implying $p = 2.35$, is marginally consistent with the theoretical Jeans stellar mass (Tab. 5). On the other hand, the occurrence of stellar wind would reduce oxygen nucleosynthesis by a factor of about 2.5 (e.g., Wang and Silk, 1993) which, in turn, would raise the lower mass limit of long-lived stars, provided the (true) yield remains unchanged (e.g., C07, Appendix C).

Within the current model, the lower mass limit of long-lived stars is related to a power-law IMF where $2.35 \leq p \leq 2.9$ provides a poor fit to low ($\tilde{m} < 1$) masses (e.g., Tinney, 1993; Burrows et al., 1993; Binney, 1999; Weidner and Kroupa, 2005). In particular, the number of low-mass stars is overestimated by a power-law IMF in comparison with current observations. The real and the power-law IMF, $\phi(\tilde{m}) = \tilde{m}^{-p}$, can be constrained to yield the same mass in a star generation, as:

$$\int_{(\tilde{m}_{mf})_{\text{real}}}^{\tilde{m}_{Mf}} \tilde{m} \Phi_{\text{real}}(\tilde{m}) d\tilde{m} = \frac{\tilde{m}_{Mf}^{2-p} - \tilde{m}_{mf}^{2-p}}{2-p} ; \quad (42a)$$

$$(\tilde{m}_{mf})_{\text{real}} \leq \tilde{m}_{mf} ; \quad (42b)$$

where \tilde{m}_{Mf} is the upper mass limit of formed stars. Accordingly, the parameter, m_{mf} , related to a power-law IMF, has to be conceived as an effective

lower mass limit of long-lived stars.

The more relevant parameters of inhomogeneous simple models related to halo and bulge (C07), halo-like thick disk, bulge-like thick disk, and thin disk, are listed in Table 8. The related values are taken from C07 (Table 9, models H1 and B1), and Table 7 (models HK1, BK1, and DN1), respectively. An universal power-law IMF is assumed, which makes no change in value of the physical parameters, \hat{p} , α , and m_{mf} . Negative values of inhibition parameter, κ , and final (inhibiting star formation) gas mass fraction, D_f , related to the bulge, correspond to enhanced instead of inhibited star formation. For further details refer to earlier work (C07).

For active regions, the probability of star formation is $\chi \lesssim 1$ for the halo, $\chi < 1$ for the bulge, and $\chi \ll 1$ for both the thick and the thin disk. Accordingly, the gas mass fraction remaining at the end of each step, μ'_R , is close to zero for the halo, about one seventh for the bulge, one fifth-one fourth for the thick disk, and one third for the thin disk. The effective yield, \hat{p}'' , is about twice larger in the thin disk (where it coincides with the true yield) than in the bulge-like thick disk; ten times than in the halo-like thick disk; five times than in the halo; (where gas is partially inhibited from forming stars); and about two thirds lower than in the bulge (where star formation is enhanced by inflowing gas with same composition as the preexisting gas; for further details refer to C07).

For the whole system, a similar trend occurs. The ratio of gas mass fraction at the end and at the beginning of a step is $q \ll 1$ for the halo, $q < 1$ for the bulge, and $q \lesssim 1$ for both the thick and the thin disk. Accordingly, the (allowing star formation) gas mass fraction remaining at the end of the evolution, μ_f , is close to zero for the halo, about four thousandths for the bulge, three quarters for the halo-like thick disk, one half for the bulge-like thick disk, and one third for the thin disk. The effective yield, \hat{p}' , is about three times larger in the thin disk (where it is due to inhomogeneous star formation) than in the bulge-like thick disk; a dozen times than in the halo-like thick disk; eighty times than in the halo; (where it is due to both inhomogeneous star formation and inhibition from forming stars); and about three fifths lower than in the bulge (where it is due to both inhomogeneous star formation and enhanced star formation; for further details refer to C07). At the end of evolution, it remains about 18% of long-lived stars (including stellar remnants) and 82% of gas inhibited from forming stars in the halo; about 72% of long-lived stars from primeval gas and 28% from inflowed gas in the bulge (with respect to the final mass, while mass fractions listed in Table 8 are related to the initial mass); about 0.3% of long-lived stars, 74% of (allowing star formation) gas, and 23% of (inhibiting star formation) gas

Table 8: Comparison between parameters of inhomogeneous simple models, related to the Galactic halo and bulge (C07, Table 9, cases H1 and B1), halo-like thick disk, bulge-like thick disk, and thin disk (Table 7, cases HK1, BK1, and DN1). An universal power-law initial mass function (IMF) is assumed in all cases, which leaves other parameters i.e. \hat{p} , α , and m_{mf} , unchanged. Gas and star mass fractions, μ_f , D_f , and s_f , are related to the initial mass with regard to the bulge, where total mass conservation is violated by gas inflow (C07). Caption of parameters: χ - probability of a region being active; μ'_R - (allowing star formation) gas mass fraction within an active region at the end of a step; q - effective gas mass fraction within a region at the end of a step; κ - ratio of gas mass fraction which inhibits star formation to long-lived star and stellar remnant mass fraction (inhibition parameter); μ_f - (allowing star formation) gas mass fraction at the end of evolution; D_f - (inhibiting star formation) gas mass fraction at the end of evolution; s_f - long-lived star mass fraction at the end of evolution; $\hat{p}''/(Z_{\odot})_{\odot}$ - effective oxygen yield related to inhibited or enhanced star formation, normalized to the solar oxygen abundance; $\hat{p}'/(Z_{\odot})_{\odot}$ - effective oxygen yield related to both inhomogeneous star formation and inhibited or enhanced star formation, normalized to the solar oxygen abundance.

parameter	value				
	halo	bulge	halo-like thick disk	bulge-like thick disk	thin disk
χ	$9.5579 \cdot 10^{-1}$	$8.7545 \cdot 10^{-1}$	$9.3147 \cdot 10^{-2}$	$1.9961 \cdot 10^{-1}$	$7.6765 \cdot 10^{-2}$
μ'_R	$8.2201 \cdot 10^{-4}$	$1.4139 \cdot 10^{-1}$	$2.3356 \cdot 10^{-1}$	$2.1579 \cdot 10^{-1}$	$3.7148 \cdot 10^{-1}$
q	$4.4991 \cdot 10^{-2}$	$2.4833 \cdot 10^{-1}$	$9.2861 \cdot 10^{-1}$	$8.4346 \cdot 10^{-1}$	$9.5175 \cdot 10^{-1}$
κ	4.5169	$-3.2099 \cdot 10^{-1}$	7.8271	1.0370	0.0000
μ_f	$4.0973 \cdot 10^{-6}$	$3.8030 \cdot 10^{-3}$	$7.4358 \cdot 10^{-1}$	$5.0613 \cdot 10^{-1}$	$2.9047 \cdot 10^{-1}$
D_f	$8.1874 \cdot 10^{-1}$	$-4.7094 \cdot 10^{-1}$	$2.2737 \cdot 10^{-1}$	$2.5142 \cdot 10^{-1}$	0.0000
s_f	$1.8126 \cdot 10^{-1}$	1.4671	$2.9049 \cdot 10^{-2}$	$2.4245 \cdot 10^{-1}$	$7.0953 \cdot 10^{-1}$
$\hat{p}''/(Z_{\odot})_{\odot}$	$1.3363 \cdot 10^{-1}$	1.0857	$8.3518 \cdot 10^{-2}$	$3.6191 \cdot 10^{-1}$	$7.3722 \cdot 10^{-1}$
$\hat{p}'/(Z_{\odot})_{\odot}$	$5.3452 \cdot 10^{-3}$	$7.6001 \cdot 10^{-1}$	$3.8418 \cdot 10^{-2}$	$1.6648 \cdot 10^{-1}$	$4.4233 \cdot 10^{-1}$

in the halo-like thick disk; about 24% of long-lived stars, 51% of (allowing star formation) gas, and 25% of (inhibiting star formation) gas in the bulge-like thick disk; about 71% of long-lived stars and 29% of gas allowing star formation in the thin disk.

The TDMD related to both homogeneous and inhomogeneous simple models provides an acceptable fit to the EDMD related to the thick disk, the thick + thin disk, (Figs. 6 and 9; upper and lower panels, respectively) and the Galaxy (Figs. 7 and 10): in particular, a non monotonic trend is reproduced. While models assume that star formation at the beginning of the evolution of each subsystem starts abruptly with constant efficiency, the data seem to indicate a somewhat gradual rate, with increasing efficiency. In other words, the occurrence of some physical process (not necessarily gas infall) seems to inhibit star formation in early times of evolution. Accordingly, the history of each Galactic subsystem (halo, bulge, halo-like thick disk, bulge-like thick disk, thin disk) could be conceived as made of two distinct phases, namely (i) assembling, where (long-lived) star formation efficiency is gradually increasing, and (ii) stabilization, where (long-lived) star formation efficiency maintains constant.

The assumption that the EDMD of the local disk is representative of the global disk, even if in contrast with an inside-out disk formation, can be considered as a useful zero-th order approximation. On the other hand, nearby stars older than about 0.2 Gyr come from birth sites which span a large range in Galactocentric distances (e.g., Rocha-Pinto et al., 2000). The orbital diffusion coefficient deduced from the observed increase of velocity dispersion with age implies that presently local stars have suffered a rms azimuthal drift from about 2 kpc (for an age of 0.2 Gyr) to many Galactic orbits (for an age of 10 Gyr); for further details refer to earlier work (Wielen, 1977). Considerable, but smaller, drift should occur also on the radial direction. In this sense, the star formation rate inferred for nearby stars is a measure of the global Milky Way star formation rate, at least at the sun Galactocentric radius (Rocha-Pinto et al., 2000), according to the estimates of the diffusion coefficient (e.g., Meusinger et al., 1991).

As outlined in an earlier attempt (Wang and Silk, 1993), radial flows of the gas (possibly due to the observed spiral density waves) or different disk star formation histories (with time scales comparable to that of chemical evolution) between the inner end the outer parts of the Galaxy, may change the local abundances, but the overall abundance in the disk should not be affected as long as there is no gain or loss of material in the disk. It can also be noticed (Wang and Silk, 1993) that the average oxygen abundance in the disk is roughly the solar value, and can be plausibly explained by the standard Scalo IMF with lower and upper star mass limit, $\tilde{m}_{mf} = 0.1$ and

$\widetilde{m}_{Mf} = 60$, respectively, or by a power-law IMF with exponent, p , within the range, $2.35 \leq p \leq 2.9$, and the same \widetilde{m}_{mf} and \widetilde{m}_{Mf} . For further details refer to the parent paper (Wang and Silk, 1993).

At the end of halo-like and bulge-like thick disk evolution, the fractional gas and star mass predicted by the model are:

$$\frac{(M_{\text{UK}})_{\text{gas}}}{(M_{\text{UK}})_o} = (\mu_{\text{UK}})_f + (D_{\text{UK}})_f ; \quad \text{U} = \text{H, B} ; \quad (43)$$

$$\frac{(M_{\text{UK}})_{\text{stars}}}{(M_{\text{UK}})_o} = (s_{\text{UK}})_f ; \quad \text{U} = \text{H, B} ; \quad (44)$$

where $(M_{\text{HK}})_o$ and $(M_{\text{BK}})_o$ are the initial halo-like and bulge-like thick disk mass, respectively. The combination of Eqs. (43) and (44) yields:

$$(M_{\text{UK}})_{\text{gas}} = \frac{(\mu_{\text{UK}})_f + (D_{\text{UK}})_f}{(s_{\text{UK}})_f} (M_{\text{UK}})_{\text{stars}} \quad \text{U} = \text{H, B} ; \quad (45)$$

where $(M_{\text{HK}})_{\text{stars}}$ and $(M_{\text{BK}})_{\text{stars}}$ must be equal to the current halo-like and bulge-like thick disk mass, respectively.

For models HK1-2, BK1-2, the values of fractional masses, $(\mu_{\text{UK}})_f$, $(D_{\text{UK}})_f$, and $(s_{\text{UK}})_f$, are listed in Table 7, and taking a current halo-like thick disk mass, $M_{\text{HK}} = (M_{\text{HK}})_{\text{stars}} = (9/296)(29/55)M_{10} \approx 0.016M_{10}$, and a current bulge-like thick disk mass, $M_{\text{BK}} = (M_{\text{BK}})_{\text{stars}} = (287/296)(29/55)M_{10} \approx 0.511M_{10}$, according to Eqs. (13b) and (14), it is found the following:

$$(M_{\text{HK}})_{\text{gas}} = 0.5359 - 0.2705M_{10} ; \quad (46)$$

$$(M_{\text{BK}})_{\text{gas}} = 1.5974 - 1.3351M_{10} ; \quad (47)$$

$$(M_{\text{DK}})_{\text{gas}} = 2.1333 - 1.6056M_{10} ; \quad (48)$$

where $(M_{\text{DK}})_{\text{gas}} = (M_{\text{HK}})_{\text{gas}} + (M_{\text{BK}})_{\text{gas}}$ is the thick disk gas mass budget available for the thin disk formation, which amounts to about 36%-28% of the assumed thin disk mass, Eq. (13b).

The above discrepancy could be avoided, taking into consideration mass loss during the thick disk evolution, in the sense that gas flows away but chemical evolution therein occurs as in the remaining gas. Accordingly, Eqs. (43)-(45) still hold but the star mass at the end of halo-like and bulge-like thick disk evolution is related to current halo-like and bulge-like thick disk mass, as:

$$(M_{\text{UK}})_{\text{stars}} = \frac{M_{\text{UK}}}{1 - f_{\text{U}}} ; \quad \text{U} = \text{H, B} ; \quad (49)$$

where $(M_{\text{UK}})_{\text{stars}}$ includes stars both inside and outside the thick disk, and f_{H} , f_{B} , are the star mass fraction outside the halo-like and bulge-like thick disk, respectively.

The boundary conditions to the problem under discussion are:

$$(M_{\text{HK}})_{\text{gas}} = M_{\text{BK}} + M_{\text{ND}} \quad ; \quad (50)$$

$$(M_{\text{BK}})_{\text{gas}} = M_{\text{ND}} \quad ; \quad (51)$$

the gas mass budget at the end of the halo-like and bulge-like thick disk must necessarily equal the bulge-like thick disk + thin disk and the thin disk mass, respectively, in absence of mass loss outside the disk.

The combination of Eqs. (45), (49), (50), and (51) yields:

$$\frac{\delta_{\text{HU}} M_{\text{BK}} + M_{\text{ND}}}{M_{\text{UK}}} (1 - f_{\text{U}}) = \frac{(\mu_{\text{UK}})_f + (D_{\text{UK}})_f}{(s_{\text{UK}})_f} \quad ; \quad \text{U} = \text{H, B} \quad ; \quad (52)$$

where δ_{ij} is the Kronecker symbol. Then the halo-like and bulge-like thick disk mass fraction to be lost during the evolution is:

$$f_{\text{U}} = 1 - \frac{(\mu_{\text{UK}})_f + (D_{\text{UK}})_f}{(s_{\text{UK}})_f} \frac{M_{\text{UK}}}{\delta_{\text{HU}} M_{\text{BK}} + M_{\text{ND}}} \quad ; \quad \text{U} = \text{H, B} \quad ; \quad (53)$$

which, for models HK1-2, BK1-2, and mass values prescribed by Eqs. (13b) and (14), reads:

$$f_{\text{H}} = 0.9074 - 0.9532 \quad ; \quad (54)$$

$$f_{\text{B}} = 0.6970 - 0.7468 \quad ; \quad (55)$$

where it can be seen that more than 90% of the halo-like thick disk initial gas budget and more than 69% of the bulge-like thick disk initial gas budget were removed from their reservoirs during the evolution. In other words, the bulge-like thick disk and the thin disk did not begin to start abruptly, but were gradually assembled during the evolution of their precursors, as inferred from the features of the EDMD mentioned above.

The results found in the current paper rely on the assumption of universal IMF, but the method used here can be generalized to the case where different IMFs in space and/or time are considered. To this aim, it is sufficient to realize that the relation, $M_i = \bar{m}_i N_i$, with regard to i -th subsystem, holds for different mean stellar masses, \bar{m}_i , related to different IMFs. Accordingly, Eq. (9) has to be generalized as $N_i/N = (\bar{m}/\bar{m}_i)(M_i/M)$, where \bar{m} is the mean stellar mass within the system. Different IMFs during the assembling and stabilization phase have been considered since a long time (e.g., Schmidt, 1963; Caimmi, 1978a,b, 1981, 1982; C00).

A different IMF in the bulge, with respect to the disk, has recently been advocated for explaining the giant star metal distribution in both the Milky

Way and Andromeda bulge (Ballero et al., 2007a), contrary to what has been found for the Milky Way bulge (C07). This discrepancy could be owing to two orders of reasons, namely: (i) instantaneous mixing has been assumed for chemical evolution in the former case and instantaneous recycling in the latter and, (ii) the cumulative metallicity distribution has been used in the former case and the differential metallicity distribution in the latter. In addition, different input parameters have been used for the related models. A comparison between observations and model predictions with regard to $[\alpha/\text{Fe}]$ ratios (e.g., Ballero et al., 2007b), cannot be performed in the framework of the model used here, as only oxygen chemical evolution is considered. Nevertheless, it is worth mentioning that Fe production mainly depends on type Ia supernovae which, in turn, have binary star progenitors. Then different IMFs in different subsystems could be mimicked by different amounts of binary star fractions.

The results found in the current paper also rely on the assumed $[\text{O}/\text{H}]$ - $[\text{Fe}/\text{H}]$ relation, Eqs.(1)-(2). Data from recent investigations, different for different Galactic subsystems (e.g., Bensby et al., 2004; Jonsell et al., 2005; Fulbright et al., 2005; Garcia Perez et al., 2006; Melendez et al., 2006; Ramirez et al., 2007) yield $[\text{O}/\text{H}]$ - $[\text{Fe}/\text{H}]$ relations lying between their counterparts expressed by Eqs. (1) and (2) which, in turn, allow comparison with earlier results related to the halo (C01), the bulge (C07), and the Galactic spheroid (C07). On the other hand, the method used in the current paper holds regardless from the assumed (or not) $[\text{O}/\text{H}]$ - $[\text{Fe}/\text{H}]$ relation.

Although direct $[\text{O}/\text{H}]$ values are available from recent observations, still they cannot be used for the global EDMD in absence of their counterparts related to each Galactic subsystem. For instance, a thick disk sample investigated by Reddy et al. (2006) is biased towards low-metallicity objects similarly to the WG95 sample; a sample investigated by Ramirez et al. (2007), hereafter quoted as the RA07 sample, is made of $N = 523$ nearby stars belonging to the halo, the thick disk, and the thin disk, within a metallicity range, $-1.5 \leq [\text{Fe}/\text{H}] \leq 0.5$. Distinct and homogeneous samples representative of the halo, the bulge, the thick disk, and the thin disk, where oxygen abundance is directly inferred, would considerably improve the results.

Nevertheless, an indicative comparison between the EDMD deduced for the thick + thin disk can be made, with regard to the FS07 sample (Fig. 3, bottom panels, crosses), and the RA07 sample where oxygen abundance was directly inferred both in presence and in absence of the LTE approximation (Ramirez et al., 2007, Table 6, available at the CDS). The local thermodynamic equilibrium (LTE) approximation well holds deep in the stellar photosphere, and a continuous transition occurs up to complete non-equilibrium (NLTE) high in the atmosphere. For further details refer to specialistic

Table 9: The empirical, differential metallicity distribution (EDMD), deduced from the RA07 sample ($N = 523$), both in presence (LTE) and in absence (NLTE) of the LTE approximation.

[O/H]	ϕ	$\Delta^\mp\phi$	LTE				NLTE			
			ψ	$\Delta^-\psi$	$\Delta^+\psi$	ΔN	ψ	$\Delta^-\psi$	$\Delta^+\psi$	ΔN
-1.2	0.064	0.007				0	-0.882	∞	0.301	1
-1.1	0.080	0.009				0				0
-1.0	0.101	0.012	-1.082	∞	0.301	1				0
-0.9	0.127	0.015				0	-1.182	∞	0.301	1
-0.8	0.160	0.018				0	-1.282	∞	0.301	1
-0.7	0.201	0.023	-1.382	∞	0.301	1	-0.683	0.257	0.161	5
-0.6	0.253	0.029	-1.005	0.374	0.198	3	-1.181	0.533	0.232	2
-0.5	0.318	0.036	-1.105	0.374	0.198	3	-0.627	0.176	0.125	9
-0.4	0.401	0.046	-0.837	0.206	0.139	7	-0.403	0.113	0.090	19
-0.3	0.505	0.058	-0.636	0.135	0.103	14	-0.250	0.082	0.069	34
-0.2	0.635	0.073	-0.539	0.104	0.084	22	-0.001	0.053	0.047	76
-0.1	0.800	0.092	-0.176	0.058	0.051	64	-0.027	0.048	0.044	90
-0.0	1.007	0.115	-0.044	0.044	0.040	109	-0.104	0.047	0.042	95
0.1	1.267	0.145	-0.129	0.043	0.039	113	-0.213	0.048	0.043	93
0.2	1.595	0.183	-0.269	0.045	0.041	103	-0.489	0.059	0.052	62
0.3	2.009	0.230	-0.626	0.062	0.054	57	-0.950	0.093	0.076	27
0.4	2.529	0.290	-1.139	0.104	0.084	22	-1.637	0.206	0.139	7
0.5	3.183	0.365	-2.281	0.533	0.232	2	-2.582	∞	0.301	1
0.6	4.008	0.459	-2.381	0.533	0.232	2				0

textbooks (e.g., Gray, 2005, Chap.6). The related EDMD, obtained by use of Eqs. (3)-(6), is listed in Table 9 both in presence (LTE) and in absence (NLTE) of the LTE approximation. Halo contamination may safely be neglected except at low metallicities, where the global contribution is also negligible in that (i) the halo star subsample in the RA07 sample is by far incomplete, and (ii) the metal-weak thick disk ($[\text{Fe}/\text{H}] \leq -1$) has not been considered therein. For further details refer to the parent paper (Ramirez et al., 2007).

The EDMD deduced from the RA07 sample and listed in Table 9, is compared in Fig.11 with its counterpart related to the thick + thin disk, plotted in Fig. 3 (bottom panels, crosses), both in presence and in absence of

the LTE approximation in the former case, and [O/Fe] plateau in the latter. The low-metallicity tail is zoomed in bottom panels. It is apparent that using the LTE approximation underestimates the EDMD for subsolar oxygen abundances and overestimates for supersolar oxygen abundances.

Although the EDMD related to the thick + thin disk (Fig. 3, bottom panels, crosses) is systematically lower for low oxygen abundances and higher for intermediate values (ending at $\phi \approx 1.56$) with respect to the EDMD deduced from the RA07 sample both in presence (triangles) and in absence (diamonds) of the LTE approximation, still a similar trend is exhibited.

A closer agreement could occur in the low-metallicity range after removing halo contamination in the RA07 sample or, alternatively, what in the current paper has been defined as the “halo-like thick disk” could be due to halo contamination in the CB00 sample. In any case, the RA07 sample cannot be considered as representative of the metal-weak ($[\text{Fe}/\text{H}] \lesssim -1$) thick disk, as mentioned above. The discrepancy in the intermediate-metallicity range is reduced in absence of the LTE approximation, and further (slightly) reduced in presence of [Fe/H] plateau (left panels), with the exception of the more metal-rich ($\phi \approx 1.56$) bin in the disk EDMD, which is related to the more metal-rich bin in the RM96 sample. Accordingly, the RM96 sample could be biased towards high metallicities, and the above mentioned bin have little statistical meaning (e.g., Haywood, 2001). In conclusion, the disk EDMD plotted in Fig. 3 (bottom panels) may be considered as acceptable to a first extent.

The empirical age-metallicity relation (EAMR), taken from a subsample ($N = 223$) of the RA07 sample, is plotted in Figs. 12 and 13 in presence and in absence of the LTE approximation, respectively. Also represented therein is the temporal behaviour of (allowing star formation) gas oxygen abundance, normalized to the solar value, related to models H1 (C07, Table 9; dashed lines), HK1 (Table 7; dotted lines), BK1 (dash-dotted lines), and DN1 (full lines). The curves correspond to the special case of constant star formation rate within active regions but, in any case, the extreme points related to the beginning and the end of a step, are left unchanged. Then the curves may be considered as representative of a time-dependent star formation rate.

It is worth recalling that simple models of chemical evolution used in the current paper are time-independent, with regard to the TDMD. Accordingly, the initial and the final time, together with the time step in the case of inhomogeneous models, can be selected for best fitting the EAMR.

For the halo, according to C07, initial and final values, $([\text{O}/\text{H}], T/\text{Gyr}) = (-3, 12.5)$ and $(0, 8.0)$, respectively, have been chosen, together with a time step, $\Delta T/\text{Gyr} = 1.125$, which implies four steps during the evolution. The initial and final values of fractional oxygen abundance, $(\phi_\ell, \Delta^* \phi'_R)$, at any step,

are (0.001, 0.9502), (0.0176, 0.9668), (0.0342, 0.9834), (0.0508, 1), corresponding to constant increments, $\Delta^*\phi = \phi_\ell - \phi_{\ell-1} = 0.01658$ and $\Delta^*\phi'_R = 0.9492$. The related TAMR is represented by four (the first out of scale) dashed lines in Figs. 12 and 13. Owing to the logarithmic scale on the horizontal axis, $\log \phi = [\text{O}/\text{H}]$, the ending point of each step is very close to $[\text{O}/\text{H}] = 0$, but only the last step actually ends therein. The starting point of each step is out of scale on the left.

For the halo-like thick disk, initial and final values, $([\text{O}/\text{H}], T/\text{Gyr}) = (-1.52, 11.0)$ and $(-0.80, 10.2)$, respectively, have been chosen, together with a time step, $\Delta T/\text{Gyr} = 0.2$, which implies four steps during the evolution. The initial and final values of fractional oxygen abundance, $(\phi_\ell, \Delta^*\phi'_R)$, at any step, are (0.03, 0.1515), (0.03285, 0.1543), (0.03569, 0.1572), (0.03854, 0.16), corresponding to constant increments, $\Delta^*\phi = \phi_\ell - \phi_{\ell-1} = 0.002846$ and $\Delta^*\phi'_R = 0.1215$. The related TAMR is represented by four dotted lines in Figs. 12 and 13. The starting point of each step is out of scale on the left.

For the bulge-like thick disk, initial and final values, $([\text{O}/\text{H}], T/\text{Gyr}) = (-0.80, 10.2)$ and $(-0.61, 9.0)$, respectively, have been chosen, together with a time step, $\Delta T/\text{Gyr} = 0.3$, which implies four steps during the evolution. The initial and final values of fractional oxygen abundance, $(\phi_\ell, \Delta^*\phi'_R)$, at any step, are (0.16, 0.7150), (0.1883, 0.7433), (0.2167, 0.7717), (0.2450, 0.8), corresponding to constant increments, $\Delta^*\phi = \phi_\ell - \phi_{\ell-1} = 0.002834$ and $\Delta^*\phi'_R = 0.5550$. The related TAMR is represented by four dot-dashed lines in Figs. 12 and 13. The starting point of the first step coincides with the ending point of the last step related to the halo-like thick disk.

For the thin disk, initial and final values, $([\text{O}/\text{H}], T/\text{Gyr}) = (-0.49, 10.0)$ and $(0.20, 0.0)$, respectively, have been chosen, together with a time step, $\Delta T/\text{Gyr} = 0.4$, which implies twenty-five steps during the evolution. The initial and final values of fractional oxygen abundance, $(\phi_\ell, \Delta^*\phi'_R)$, at the first five steps, are (0.325, 1.0550), (0.3469, 1.0769), (0.3687, 1.0988), (0.3906, 1.1207), (0.4125, 1.1425), corresponding to constant increments, $\Delta^*\phi = \phi_\ell - \phi_{\ell-1} = 0.02187$ and $\Delta^*\phi'_R = 0.7300$. The related TAMR is represented by five full lines in Figs. 12 and 13. The remaining twenty steps are out of scale on the bottom.

It is apparent that the TAMR related to the disk cannot provide an acceptable fit to the EAMR deduced from the RA07 sample both in presence and in absence of the LTE approximation. This is why models of chemical evolution used in the current paper have been selected to fit the FS07 sample for the thick disk and the RM96 sample for the thin disk, where a small amount of oxygen-rich (supersolar) objects were found using Eqs. (1) and (2). On the contrary, a consistent number of oxygen-rich objects is present in the RA07 sample which, on the other hand, is biased towards oxygen-poor

objects (Ramirez et al., 2007).

In the future, additional effort should be devoted in collecting representative samples of both the halo, the bulge, the halo-like and bulge-like thick disk, and the thin disk, where the oxygen abundance is directly derived (e.g., Ramirez et al., 2007) instead of being empirically deduced from iron abundance, as in Eqs. (1) and (2). Additional support to the distinction between halo-like and bulge-like thick disk could be provided from the related distributions of specific angular momentum. In particular, the former and the latter are expected to exhibit differences as in the Galactic spheroid with respect to the Galactic disk (Wyse and Gilmore, 1992; Ibata and Gilmore, 1995). It would also be important to establish if the metal-weak thick disk (e.g., Martin and Morrison, 1998; Beers et al., 2002) is the actual precursor of the metal-enriched thick disk or, on the other hand, coincides with the flattened, rotation-supported halo subsystem (Prochaska et al., 2000), or both. Further investigation will provide additional support, or contradict, the results of the current attempt.

7 Conclusion

The empirical differential metallicity distribution (EDMD) in the thick disk has been deduced from two different samples involving (WG95) local thick disk stars derived from Gliese and scaled in situ samples within the range, $-1.20 \leq [\text{Fe}/\text{H}] \leq -0.20$ (Wyse and Gilmore, 1995), and (CB00) $N = 46$ likely metal-weak thick disk stars within the range, $-2.20 \leq [\text{Fe}/\text{H}] \leq -1.00$ (Chiba and Beers, 2000). The EDMD in the thin disk has been deduced from (RM96) $N = 287$ chemically selected G dwarfs within 25 kpc from the sun, with the corrections performed in order to take into account the stellar scale height (Rocha-Pinto and Maciel, 1996). To this aim, two alternative $[\text{O}/\text{H}]-[\text{Fe}/\text{H}]$ dependences have been used, Eqs. (1) and (2), according to earlier attempts where the EDMD was deduced in halo field stars (C01), the globular cluster subsystem (C07), and the bulge (C07).

The metal-poor and metal-rich EDMD related to the thick disk, have shown analogies with their halo and bulge counterparts, respectively. For this reason, the thick disk has been conceived as made of two distinct regions: the halo-like and bulge-like thick disk, and the related EDMD has been deduced. The data have been fitted, to an acceptable extent, by both homogeneous and inhomogeneous simple models of chemical evolution. For the thin disk, only inhomogeneous models have succeeded in reproducing the data, as already shown in earlier attempts (Malinie et al., 1993; C00).

Under the assumption of an universal initial mass function (IMF) and a

value of the true yield equal to the linear fit related to the thin disk solar neighbourhood, inhibition of thick disk star formation (implying gas outflow) has been required to reproduce the EDMD. A power-law IMF has been considered, $\phi(\tilde{m}) \propto \tilde{m}^{-p}$, within the range, $2.35 \leq p \leq 2.9$, and special effort has been given to the limiting cases, (i) $p = 2.9$, which is acceptably close to Scalo (1986) IMF for $m \gtrsim m_{\odot}$, and (ii) $p = 2.35$, which is the Salpeter (1955) IMF.

The EDMD related to the disk has been determined by weighting the mass, where each distribution has been assumed to be typical for the corresponding subsystem. Following a similar procedure, the EDMD related to the Galaxy has been computed using the results of an earlier attempt (C07) with regard to the bulge and the halo. In any case, it has been inferred that a more refined model involving an initially increasing star formation efficiency (but not necessarily implying gas infall) while assembling Galactic subsystems, could provide a better agreement with the data, including the right amount of mass budget needed for the formation of the bulge-like thick disk and the thin disk. The theoretical differential metallicity distribution (TDMD) related to both homogeneous and inhomogeneous simple models has provided an acceptable fit to the EDMD related to the Galaxy and, in particular, a non-monotonic trend has been reproduced.

An indicative comparison has been performed between the EDMD deduced for the thick + thin disk both in presence and in absence of [O/Fe] plateau, and its counterpart computed for (RA07) $N = 523$ nearby ($d < 150$ pc) stars with metallicity in the range, $-1.5 < [\text{Fe}/\text{H}] < 0.5$, for which the oxygen abundance has been determined both in presence and in absence of the LTE approximation (Ramirez et al., 2007). It has been found that both distributions exhibit a similar trend, though systematic differences exist, which has made the fit acceptable to a first extent.

The empirical age-metallicity distribution (EAMR), taken from a subsample ($N = 223$) of the RA07 sample for which age determination is available (Ramirez et al., 2007), has been compared with the theoretical age-metallicity relation (TAMR), predicted by models related to the halo, the halo-like thick disk, the bulge-like thick disk, and the thin disk. The fit has shown to be unsatisfactory for the following reason. The models of chemical evolution used in the current paper have been selected to match the data from earlier samples for both the thick disk (WG95 and CB00) and the thin disk (RM96), where a small amount of oxygen-rich (supersolar) objects were found using Eqs. (1) and (2). Conversely, a consistent number of oxygen-rich objects has been found in the RA07 sample which, on the other hand, is biased towards oxygen-poor objects (Ramirez et al., 2007).

References

- [1] Adams, F.C., Fatuzzo, M., 1996. *ApJ* 464, 256.
- [2] Allende-Prieto, C., Lambert, D.L., Asplund M., 2001. *ApJ* 556, L63.
- [3] Anders, E., Grevesse, N., 1989. *Geochim. Cosmochim. Acta* 53, 197.
- [4] Asplund, M., Grevesse, N., Sauval, A.J., et al., 2004. *A&A* 417, 751.
- [5] Asplund, M., Grevesse, N., Sauval, A.J., 2005. In *Cosmic Abundances as Records of Stellar Evolution and Nucleosynthesis ASP*, ed. F.N. Bash and T.G. Barnes, 25.
- [6] Ballero, S.K., Kroupa, P., Matteucci, F., 2007a. *A&A* 467, 117.
- [7] Ballero, S.K., Matteucci, F., Origlia, L., Rich, R.M., 2007b. *A&A* 467, 123.
- [8] Barbuy, B., Nissen, P.E., Peterson, R., Spite, F. (eds.), *Proceedings of Oxygen abundances in stars and implications to nucleosynthesis and cosmology (IAU Joint Discussion 8)*, 2001. *New Astron. Rev.* 45, 509.
- [9] Beers, T.C., Drilling, J.S., Rossi, S., et al., 2002. *AJ* 124, 931.
- [10] Bensby, T., Feltzing, S., Lundström, I., 2004. *A&A* 415, 155.
- [11] Binney, J., 1999. *MNRAS* 307, L27.
- [12] Bromm, V., Loeb, A., 2003. *Nat* 425, 812.
- [13] Bromm, V., 2004. *PASP* 116, 103.
- [14] Bromm, V., Larson, R.B., 2004. *ARA&A* 42, 79.
- [15] Burrows, A., Hubbard, W.B., Saumon, D., Lunine, J.I., 1993. *ApJ* 406, 158.
- [16] Caimmi, R., 1978a. *ApSS* 59, 109.
- [17] Caimmi, R., 1978b. *ApSS* 59, 413.
- [18] Caimmi, R., 1981. *ApSS* 79, 87.
- [19] Caimmi, R., 1982. *ApSS* 84, 373.
- [20] Caimmi, R., 2000. *AN* 321, 323 (C00).

- [21] Caimmi, R., 2001a. AN 322, 65 (C00, erratum).
- [22] Caimmi, R., 2001b. AN 322, 241 (C01).
- [23] Caimmi, R., 2007. NewA 12, 289 (C07).
- [24] Carretta, E., Gratton, R., Sneden, C., 2000. A&A 356, 238.
- [25] Chiba, M., Beers, T.C., 2000. AJ 119, 2843.
- [26] Christlieb, N., Bessell, M.S., Beers, T.C., et al., 2002. Nat 419, 904.
- [27] Favata, F., Micela, G., Sciortino, S., 1997. A&A 323, 809.
- [28] Ferreras, I., Wyse, R.F.G., Silk, J., 2003. MNRAS 345, 1381.
- [29] Frebel, A., Christlieb, N., Norris, J.E., et al., 2006. ApJ 638, L17.
- [30] Fulbright J.P., Rich R.M., McWilliam A., 2005. NPA 758, 197. Available from <astro-ph/0411041>.
- [31] Garcia Perez, A.E., Asplund, M., Primas, F., et al., 2006. A&A 451, 621.
- [32] Gilmore, G., Wyse, R.F.G., Jones, J.B., 1995. AJ 109, 1095.
- [33] Gray, D.F., 2005. The Observation and Analysis of Stellar Photospheres, Cambridge University Press, UK.
- [34] Grevesse, N., Sauval, A.J., Dishoeck, E.F., 1984. A&A 141, 10.
- [35] Hartwick, F.D.A., 1976. ApJ 209, 418.
- [36] Haywood, M., 2001. MNRAS 325, 1365.
- [37] Haywood, M., 2006. MNRAS 371, 1760.
- [38] Henry, R.B.C., Worthey, G., 1999. PASP 111, 919.
- [39] Ibata, R.A., Gilmore, G.F., 1995. MNRAS 275, 605.
- [40] Israelian, G., Rebolo, R., Garcia-Lopez, R.J., et al., 2001a. ApJ 551, 833.
- [41] Israelian, G., Rebolo, R., Garcia-Lopez, R.J., et al., 2001b. ApJ 560, 535.
- [42] Iwamoto, N., Umeda, H., Tominaga, N., et al., 2005. Sci 309, 451.

- [43] Jonsell, K., Edvardsson, B., Gustafsson, B., et al., 2005. *A&A* 440, 321.
- [44] Jørgensen, B.R., 2000. *A&A* 363, 947.
- [45] Karlsson, T., 2005. *A&A* 439, 93.
- [46] Kotoneva, E., Flynn, C., Chiappini, C., Matteucci, F., 2002. *MNRAS* 336, 879.
- [47] Landi, E., Feldman, U., Doschek, G.A., 2007. *ApJ* 659, 743.
- [48] Larson, R.B., 1974. *MNRAS* 166, 585.
- [49] Larson, R.B., 2005. *MNRAS* 359, 211.
- [50] Lynden-Bell, D., 1975. *Vistas Astron.* 19, 299.
- [51] Mackey, A.D., van den Bergh, S., 2005. *MNRAS* 360, 631.
- [52] Malinie, G., Hartmann, D.H., Clayton, D.D., Mathews, G.J., 1993. *ApJ* 413, 633.
- [53] Martin, J.C., Morrison, H.L., 1998. *AJ* 116, 1724.
- [54] Melendez, J., 2004. *ApJ* 615, 1042.
- [55] Melendez, J., Shchukina, N.G., Vasiljeva, I.E., Ramirez, I., 2006. *ApJ* 642, 1082.
- [56] Meusinger, H., Stecklum, B., Reimann, H.-G., 1991. *A&A* 245, 57.
- [57] Miller, G.E., Scalo, J.M., 1979. *ApJS* 41, 513.
- [58] Nordström, B., Mayor, M., Andersen, J., et al., 2004. *A&A* 418, 989.
- [59] Oey, M.S., 2003. *MNRAS* 339, 849.
- [60] Pagel, B.E.J., 1989. The G-dwarf Problem and Radio-active Cosmochronology. In: Beckman J.E., Pagel B.E.J. (eds.) *Evolutionary Phenomena in Galaxies*, Cambridge Univ. Press, p.201.
- [61] Pagel, B.E.J., Patchett, B.E., 1975. *MNRAS* 172, 13.
- [62] Pilyugin, L.S., Edmunds, M.G., 1996. *A&A* 313, 792.
- [63] Prantzos, N., 1994. *A&A* 284, 477.
- [64] Prantzos, N., 2003. *A&A* 404, 211.

- [65] Prantzos, N., 2007. Arxiv: astro-ph/0611476.
- [66] Prantzos, N., Silk, J., 1998. ApJ 507, 229.
- [67] Prochaska, J.X., Naumov, S.O., Carney, B.W., et al., 2000. AJ 120, 2513.
- [68] Ramirez, I., Allende Prieto, C., Lambert, D.L., 2007. A&A 465, 271.
- [69] Reddy, D.E., Tomkin, J., Lambert, D.L., Allende Prieto, C., 2003. MNRAS 340, 304.
- [70] Reddy, D.E., Lambert, D.L., Allende Prieto, C., 2006. MNRAS 367, 1329.
- [71] Rocha-Pinto, H.J., Maciel, W.J., 1996. MNRAS 279, 447.
- [72] Rocha-Pinto, H.J., Scalo, J.M., Maciel, W.J., Flynn, C., 2000. ApJ 531, L115.
- [73] Ryan, S.G., Norris, J.E., 1991. AJ 101, 1865.
- [74] Sadler, E.M., Rich, R.M., Terndrup, D.M., 1996. AJ 112, 171.
- [75] Salpeter, E.E., 1955. ApJ 121, 161.
- [76] Sauval, A.J., Grevesse, N., Brault, N., et al., 1984. ApJ 282, 330.
- [77] Scalo, J.M., 1986. FCPH 11, 1.
- [78] Schmidt, M., 1963. ApJ 137, 758.
- [79] Searle, L., 1972. Star Formation and the Chemical History of Galaxies. In: Cayrel de Strobel, G., Delplace, A.M. (eds.) L'Agés des Etoiles, Observatoire de Paris-Meudon, p. 52.
- [80] Searle, L., Sargent, W.L.W., 1972. ApJ 173, 25.
- [81] Shchukina, N., Trusillo Bueno, J., Asplund, M., 2005. ApJ 618, 939.
- [82] Socas-Navarro, H., Norton, A.A., 2007. ApJ 660, L153.
- [83] Sofia, U.J., Meyer, P.M., 2001. ApJ 554, L221.
- [84] Thacker, R.J., Scannapieco, E., Davis, M., 2002. ApJ 581, 836.
- [85] Tinney, C.G., 1993. ApJ 414, 279.

- [86] van den Bergh, S., 1962. ApJ 67, 486.
- [87] Wang, B., Silk, J., 1993. ApJ 406, 580.
- [88] Weidner, C., Kroupa, P., 2005. ApJ 625, 754.
- [89] Wielen, R., 1977. A&A 60, 263.
- [90] Worthey, G., Dorman, B., Jones, L.A., 1996. AJ 112, 948.
- [91] Wyse, R.F.G., Gilmore, G., 1992. AJ 104, 144.
- [92] Wyse, R.F.G., Gilmore, G., 1995. AJ 110, 2771.

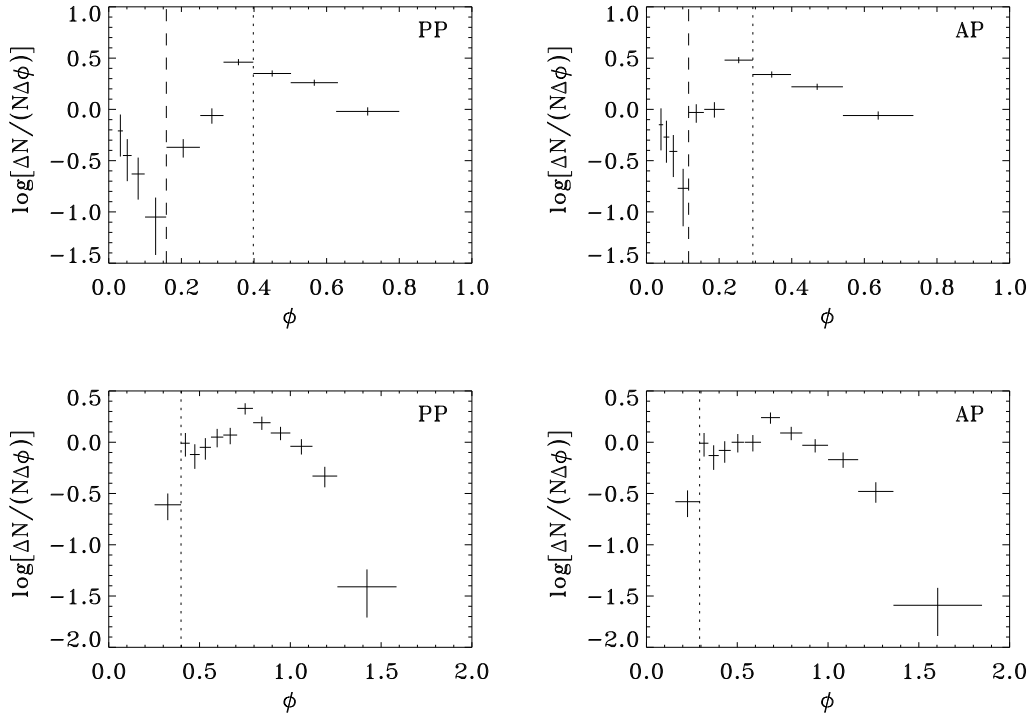


Figure 1: The empirical, differential metallicity distribution (EDMD) in thick (top panels) and thin (bottom panels) disk, both in presence (PP) and in absence (AP) of $[O/Fe]$ plateau. Plots have been deduced from the FS07 sample for the thick disk, and from the RM96 sample for the thin disk. The dotted vertical line marks the transition from halo to bulge/disk globular cluster morphological type, $[Fe/H] = -0.8$. The dashed vertical line marks the transition from halo-like to bulge-like thick disk, $[Fe/H] = -1.4$.

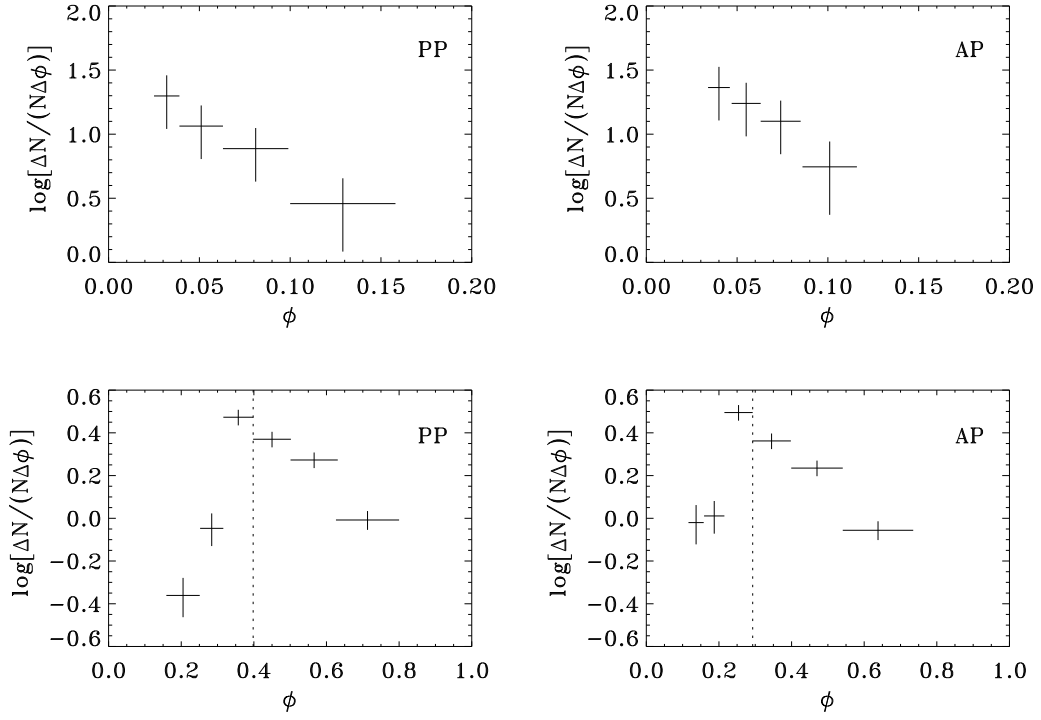


Figure 2: The empirical, differential metallicity distribution (EDMD) in halo-like (top panels) and bulge-like (bottom panels) thick disk, both in presence (PP) and in absence (AP) of [O/Fe] plateau. The dotted vertical line marks the transition from halo to bulge/disk globular cluster morphological type, $[\text{Fe}/\text{H}] = -0.8$.

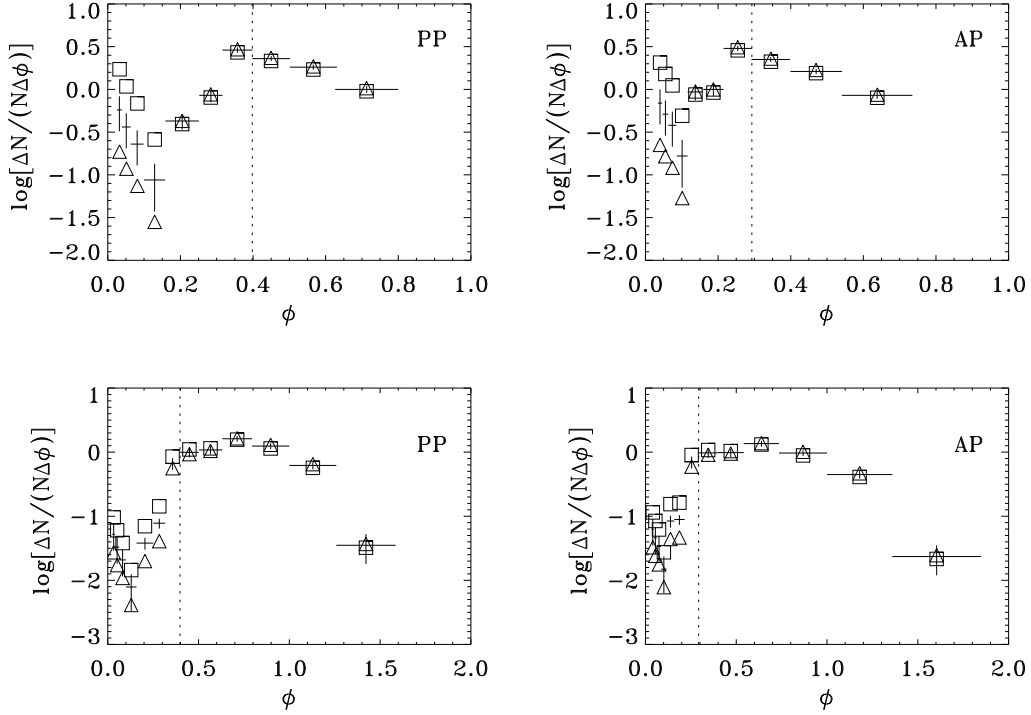


Figure 3: The empirical, differential metallicity distribution (EDMD) in halo-like + bulge-like thick disk (top panels) and halo-like + bulge-like thick + thin disk (bottom panels), both in presence (PP) and in absence (AP) of [O/Fe] plateau. Different symbols are related to different halo-like to bulge-like thick disk mass ratio, $M_{\text{HK}}/M_{\text{BK}}$, for top panels, and to different thick to thin disk mass ratio, $M_{\text{KD}}/M_{\text{ND}}$, for bottom panels. Caption of symbols: top panels, $M_{\text{HK}}/M_{\text{BK}} = 18/574$ (crosses); 0.01 (triangles); 0.10 (squares); bottom panels, $M_{\text{KD}}/M_{\text{ND}} = 0.10$ (crosses); 0.05 (triangles); 0.20 (squares). In addition, $M_{\text{HK}}/M_{\text{BK}} = 18/574 \approx 0.03136$ for bottom panels. The dotted vertical line marks the transition from halo to bulge/disk globular cluster morphological type, $[\text{Fe}/\text{H}] = -0.8$.

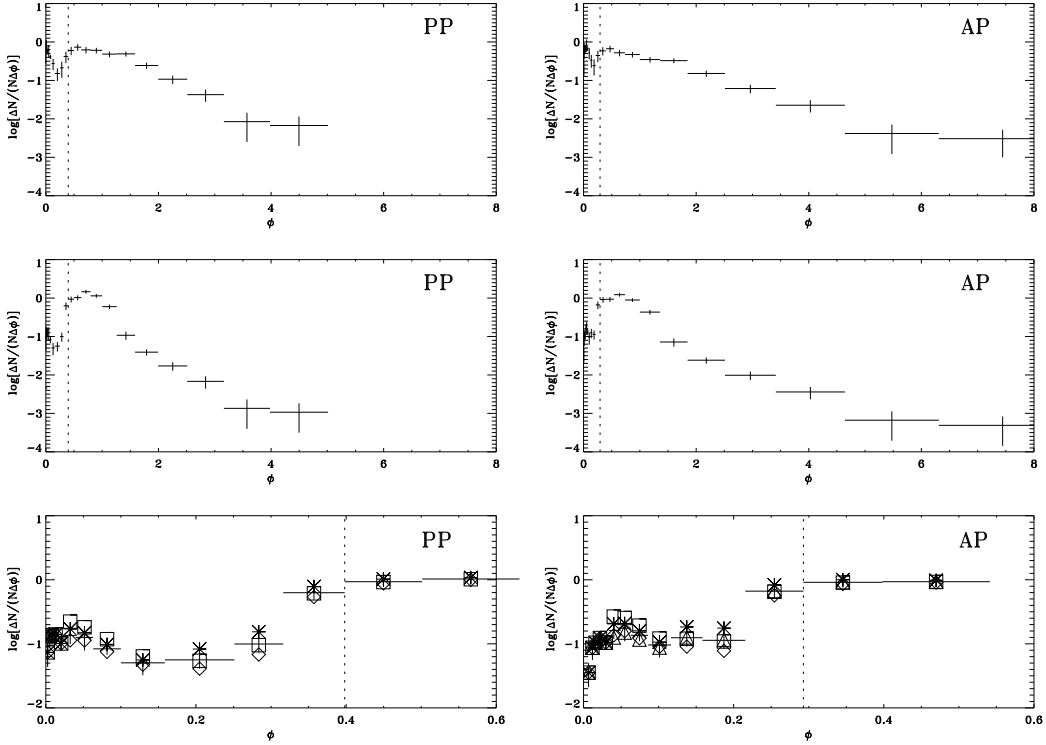


Figure 4: The empirical, differential metallicity distribution (EDMD) in the Galaxy (middle panels) for halo-like to bulge-like thick disk mass ratio, $M_{\text{HK}}/M_{\text{BK}} = 18/574$, and thick disk to thin disk mass ratio, $M_{\text{KD}}/M_{\text{ND}} = 0.1$, both in presence (PP) and in absence (AP) of [O/Fe] plateau. The EDMD in the Galactic spheroid (C07) is shown in top panels for comparison. Additional cases related to different mass ratios are also represented (bottom panels) where the error bars have been suppressed to avoid confusion. Caption of symbols: $M_{\text{HK}}/M_{\text{BK}} = 0.01$ (triangles), 0.10 (squares), where $M_{\text{KD}}/M_{\text{ND}} = 0.1$; $M_{\text{KD}}/M_{\text{ND}} = 0.05$ (diamonds), 0.20 (asterisks), where $M_{\text{HK}}/M_{\text{BK}} = 18/574$. Crosses representing error bars are related to the reference case, $M_{\text{HK}}/M_{\text{BK}} = 18/574 \approx 0.03136$ and $M_{\text{KD}}/M_{\text{ND}} = 0.10$. The dotted vertical line marks the transition from halo to bulge/disk globular cluster morphological type, $[\text{Fe}/\text{H}] = -0.8$.

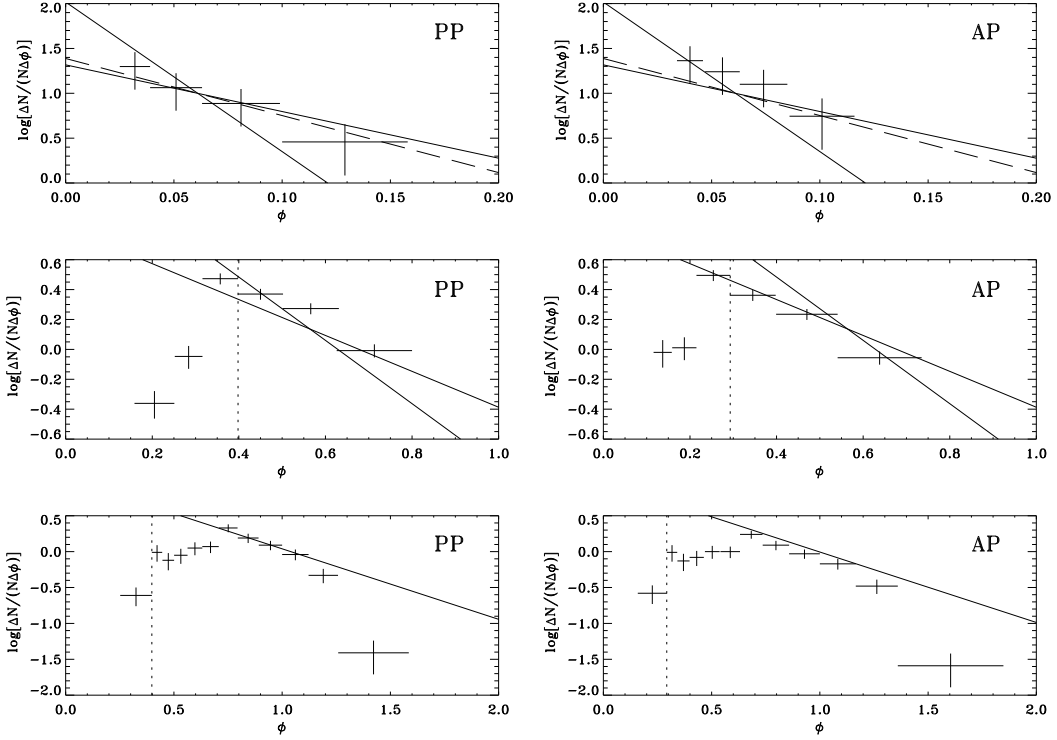


Figure 5: Comparison between theoretical (TDMD) and empirical differential metallicity distribution (EDMD) in halo-like thick disk (top panels), bulge-like thick disk (middle panels) and thin disk (bottom panels) stars, both in presence (left panels) and in absence (right panels) of $[O/Fe]$ plateau, respectively. The straight lines correspond to homogeneous models, HK1-HK2 (top panels), BK1-BK2 (middle panels), and to inhomogeneous models, DN1-DN2 (bottom panels), defined in Table 6. The dashed line in top panels (model HK2) is very close to the limiting case, $\mu_f = 0$, defined by Eqs. (18) and (19) and model HK1 is represented by the less inclined (in absolute value) full line. Accordingly, the linear fits lying between the dashed line and the more inclined (in absolute value) full line, must be excluded. Crosses represent the data and related uncertainties, as in Figs. 1-2. The dotted vertical line marks the transition from halo to bulge/disk globular cluster morphological type, $[Fe/H] = -0.8$.

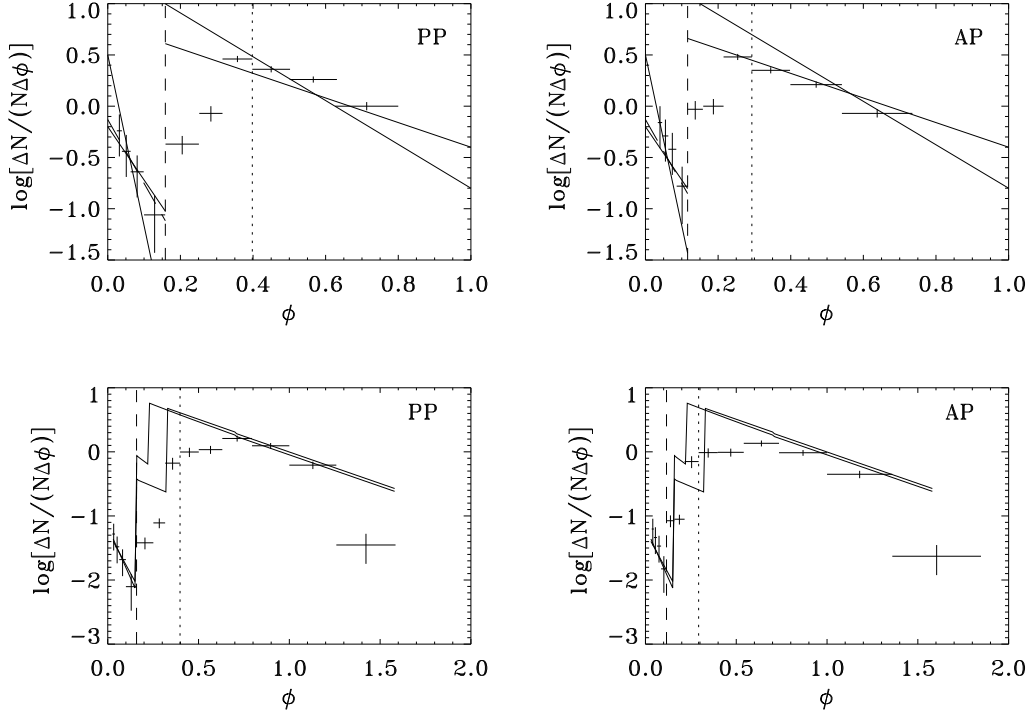


Figure 6: Comparison between theoretical (TDMD) and empirical differential metallicity distribution (EDMD) in halo-like + bulge-like thick disk (top panels) and thick + thin disk (bottom panels), both in presence (left panels) and in absence (right panels) of $[\text{O}/\text{Fe}]$ plateau, respectively. The straight lines correspond to homogeneous models, HK1-HK2 (low oxygen abundances), BK1-BK2 (intermediate oxygen abundances), and DN1-DN2 (high oxygen abundances), defined in Table 6. Crosses represent renormalized data and related uncertainties, as in Fig. 3. The dotted vertical line marks the transition from halo to bulge/disk globular cluster morphological type, $[\text{Fe}/\text{H}] = -0.8$. The dashed vertical line marks the (assumed) transition from halo-like to bulge-like thick disk.

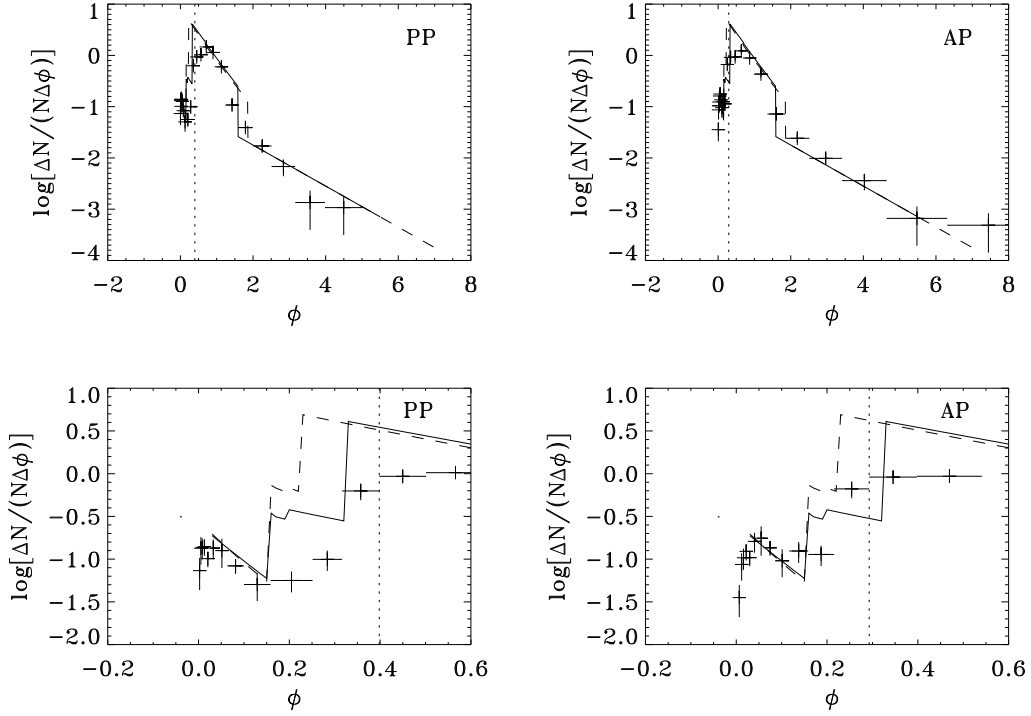


Figure 7: Comparison between theoretical (TDMD) and empirical differential metallicity distribution (EDMD) in the Galaxy (top panels) and zoomed for low oxygen abundance (bottom panels), both in presence (left panels) and in absence (right panels) of [O/Fe] plateau, respectively. The curves correspond to models H1, B1, HK1, BK1, DN1 (full); H2, B2, HK2, BK2, DN2 (dashed) defined in: C07, Tables 7 and 8 therein (H, B); Tables 5 and 6 (HK, BK, DN); all combined via Eq. (29). The dotted vertical line marks the transition from halo to bulge/disk globular cluster morphological type, $[\text{Fe}/\text{H}]=-0.8$.

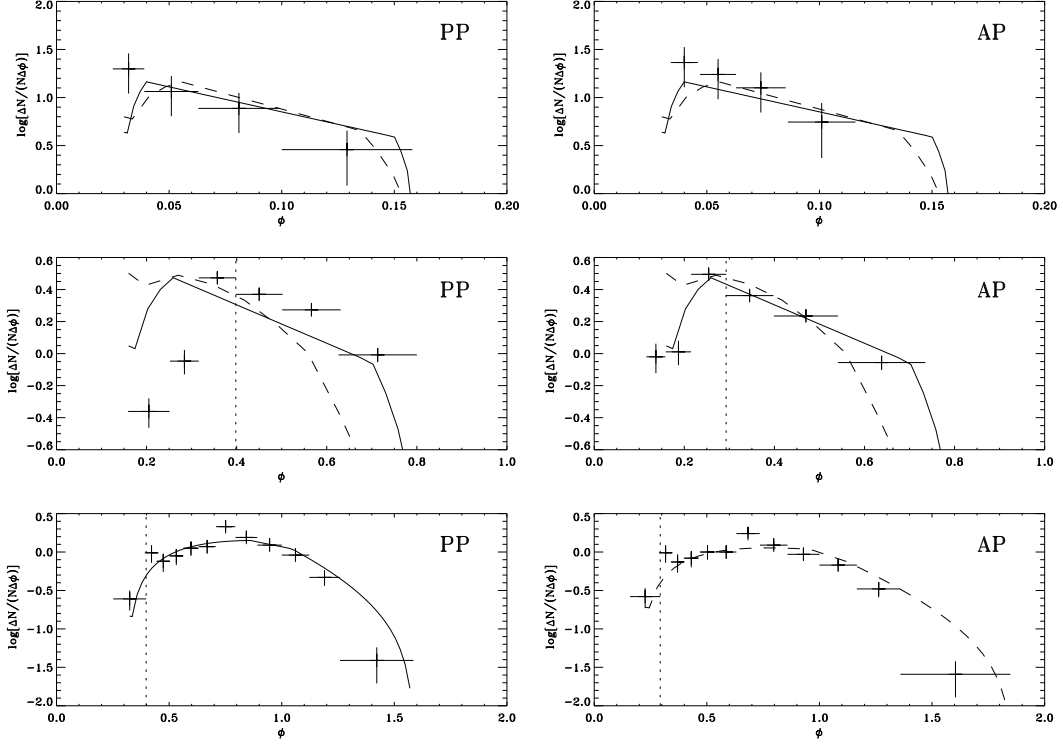


Figure 8: Comparison between theoretical (TDMD) and empirical differential metallicity distribution (EDMD) in halo-like thick disk (top panels), bulge-like thick disk (middle panels), and thin disk (bottom panels) stars, both in presence (left panels) and in absence (right panels) of $[O/Fe]$ plateau, respectively. Full curves correspond to inhomogeneous models HK1 (top panels), BK1 (middle panels), and DN1 (left bottom panel), and dashed curves to HK2 (top panels), BK2 (middle panels), and DN2 (right bottom panel), defined in Table 7. Crosses represent the data and related uncertainties, as in Figs. 1-2. The dotted vertical line marks the transition from halo to bulge/disk morphological type in globular clusters, $[Fe/H] = -0.8$.

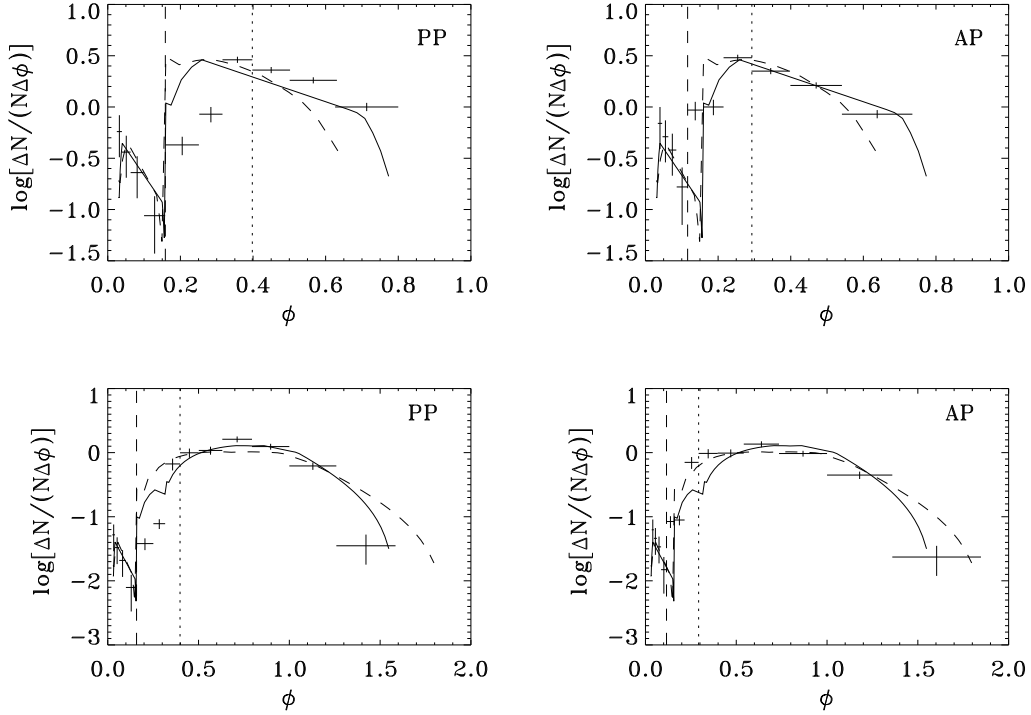


Figure 9: Comparison between theoretical (TDMD) and empirical differential metallicity distribution (EDMD) in halo-like + bulge-like thick disk (top panels) and thick + thin disk (bottom panels), both in presence (left panels) and in absence (right panels) of $[O/Fe]$ plateau, respectively. Full and dashed curves correspond to models K1, K2, (top panels), and D1, D2, (bottom panels), obtained using models HK1, BK1; HK2, BK2; (top panels); and HK1, BK1, DN1; HK2, BK2, DN2; (bottom panels); respectively, defined in Tables 5 and 7, and combined via Eqs. (9) and (28). Crosses represent the renormalized data and related uncertainties, as in Fig. 6. The dotted vertical line marks the transition from halo to bulge/disk globular cluster morphological type, $[Fe/H]=-0.8$. The dashed vertical line marks the (assumed) transition from halo-like to bulge-like thick disk.

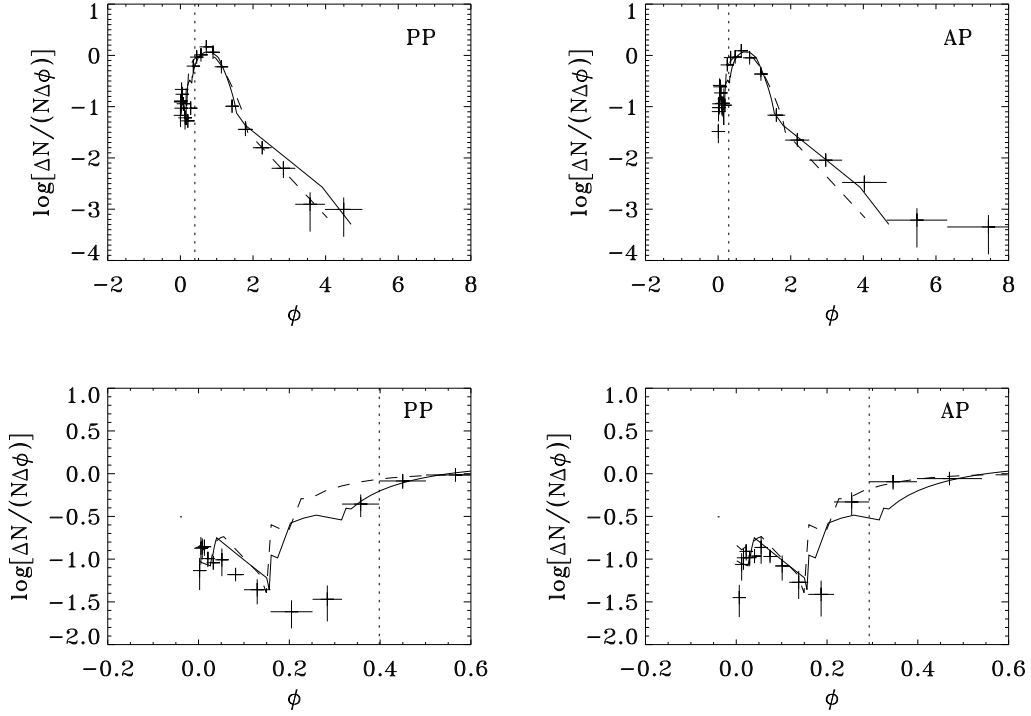


Figure 10: Comparison between theoretical (TDMD) and empirical differential metallicity distribution (EDMD) in the Galaxy (top panels) and zoomed for low normalized oxygen abundances (bottom panels), both in presence (left panels) and in absence (right panels) of $[O/Fe]$ plateau, respectively. Curves correspond to models H1, B1, HK1, BK1, DN1, (full); H2, B2, HK2, BK2, DN2, (dashed); defined in C07, Tables 7 and 9 therein (H, B) and Tables 5 and 7 (HK, BK, DN), all combined via Eqs. (9) and (28). The dotted vertical line marks the transition from halo to bulge/disk globular cluster morphological type, $[Fe/H] = -0.8$.

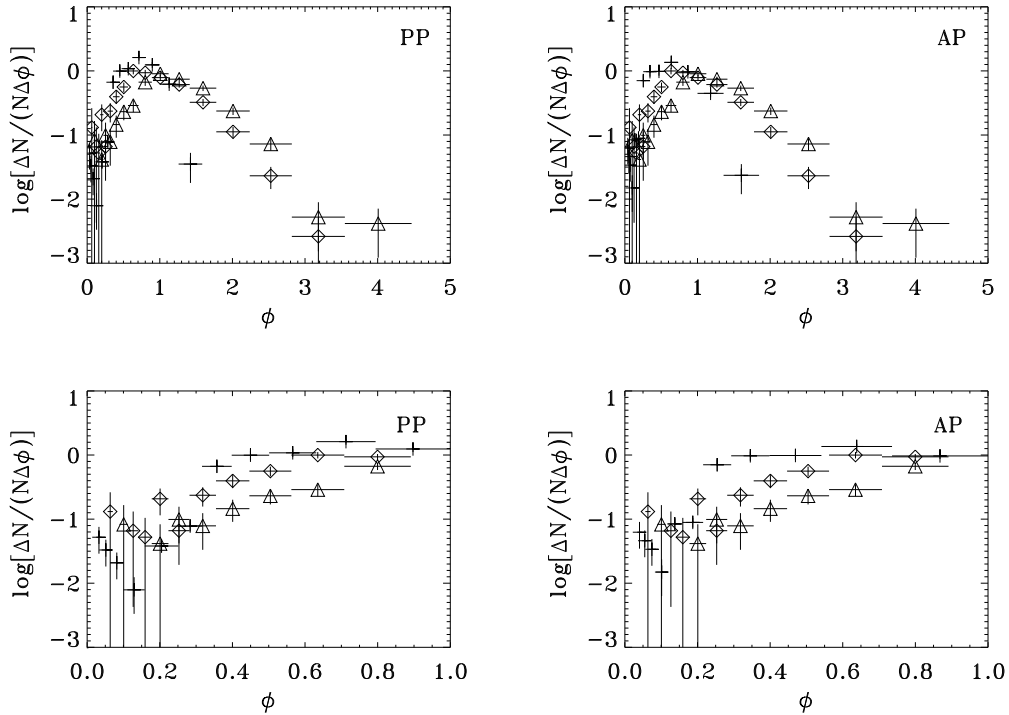


Figure 11: The empirical, differential metallicity distribution (EDMD) deduced from the RA07 sample ($N = 523$) including nearby halo (by far incomplete), thick disk, and thin disk stars, both in presence (triangles) and in absence (diamonds) of the LTE approximation. The EDMD deduced for the thick + thin disk (Fig. 3, crosses) is also represented for comparison both in presence (left panels) and in absence (right panels) of $[\text{O}/\text{Fe}]$ plateau. The low-metallicity tail is zoomed in bottom panels.

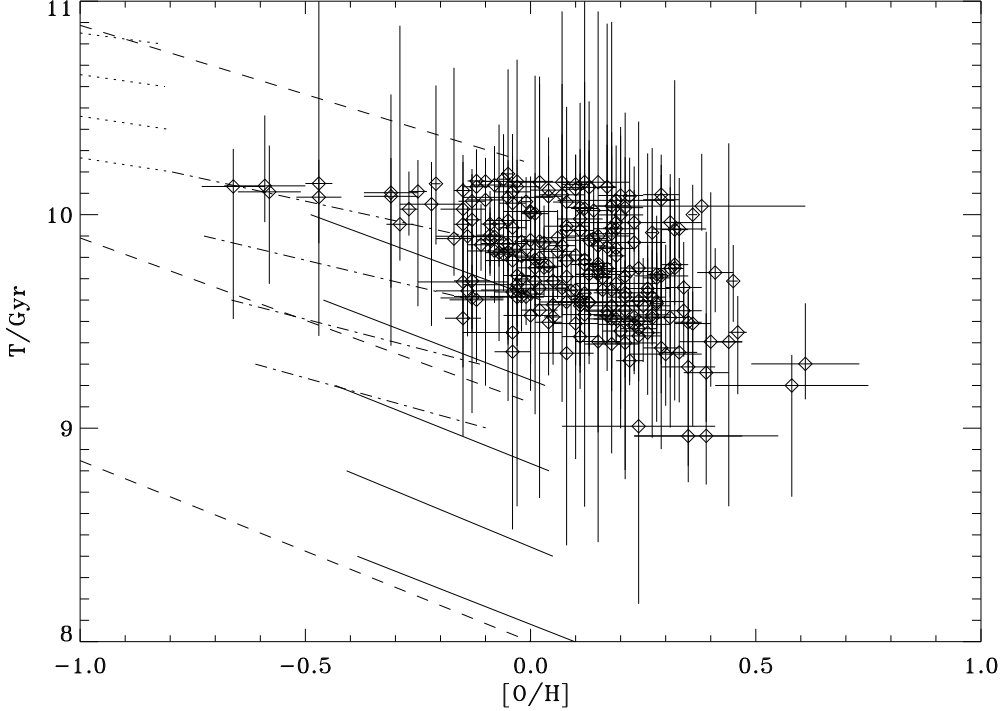


Figure 12: Comparison between the empirical (EAMR) and theoretical age-metallicity relation (TAMR) in presence of the LTE approximation. The data are from a subsample ($N = 223$) of the RA07 sample, for which ages have been determined (Ramirez et al., 2007). Dashed, dotted, dash-dotted, and full lines are related to models H1 (C07), HK1, BK1, and DN1, respectively, in the special case of constant star formation rate within active regions. The halo star formation begins at $([O/H], T/\text{Gyr}) = (-3, 12.5)$ and ends at $(0, 8.0)$, within four time steps, $\Delta T/\text{Gyr} = 1.125$ (C07). The starting point of each step is out of scale on the left; the first step is out of scale on the top; and cannot be shown. The halo-like thick disk star formation begins at $(-1.52, 11.0)$ and ends at $(-0.80, 10.2)$, within four time steps, $\Delta T/\text{Gyr} = 0.2$. The starting point of each step is out of scale on the left, and cannot be shown. The bulge-like thick disk star formation begins at $(-0.80, 10.2)$ and ends at $(-0.10, 9.0)$, within four time steps, $\Delta T/\text{Gyr} = 0.3$. The thin disk star formation begins at $(-0.49, 10.0)$ and is still continuing (in the sense that star formation occurs) up today at $(0.20, 0.0)$ within twenty-five time steps, $\Delta T/\text{Gyr} = 0.4$. The last twenty time steps are out scale on the bottom.

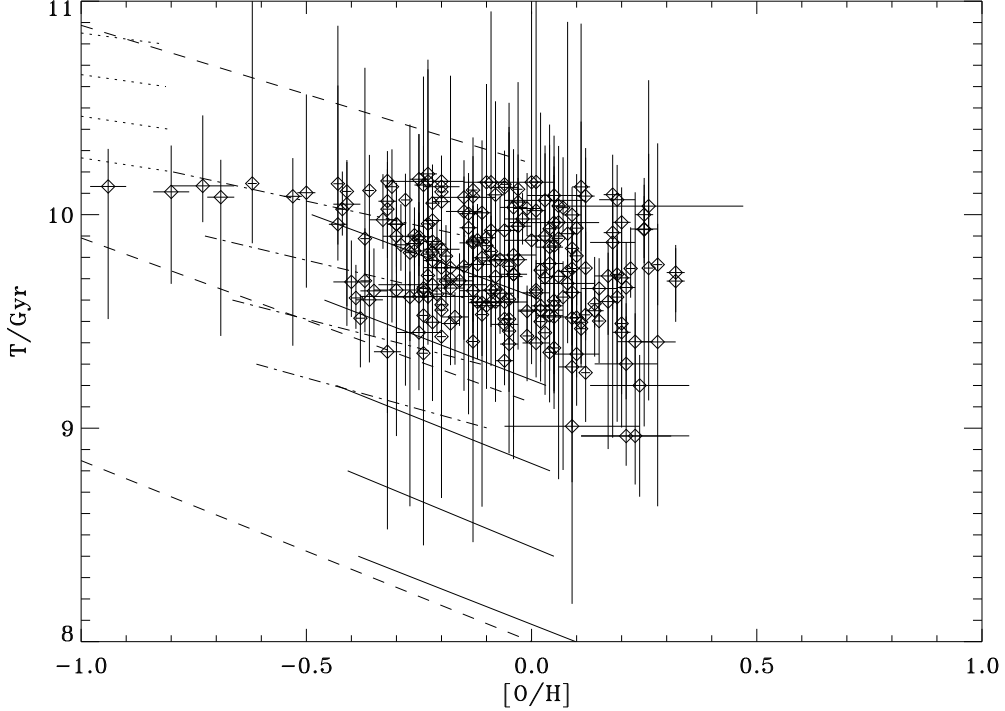


Figure 13: Comparison between the empirical (EAMR) and theoretical age-metallicity relation (TAMR) in absence of the LTE approximation. The data are from a subsample ($N = 223$) of the RA07 sample, for which ages have been determined (Ramirez et al., 2007). Dashed, dotted, dash-dotted, and full lines are related to models H1 (C07), HK1, BK1, and DN1, respectively, in the special case of constant star formation rate within active regions. The halo star formation begins at $([O/H], T/\text{Gyr}) = (-3, 12.5)$ and ends at $(0, 8.0)$, within four time steps, $\Delta T/\text{Gyr} = 1.125$ (C07). The starting point of each step is out of scale on the left; the first step is out of scale on the top; and cannot be shown. The halo-like thick disk star formation begins at $(-1.52, 11.0)$ and ends at $(-0.80, 10.2)$, within four time steps, $\Delta T/\text{Gyr} = 0.2$. The starting point of each step is out of scale on the left, and cannot be shown. The bulge-like thick disk star formation begins at $(-0.80, 10.2)$ and ends at $(-0.10, 9.0)$, within four time steps, $\Delta T/\text{Gyr} = 0.3$. The thin disk star formation begins at $(-0.49, 10.0)$ and is still continuing (in the sense that star formation occurs) up today at $(0.20, 0.0)$ within twenty-five time steps, $\Delta T/\text{Gyr} = 0.4$. The last twenty time steps are out scale on the bottom.